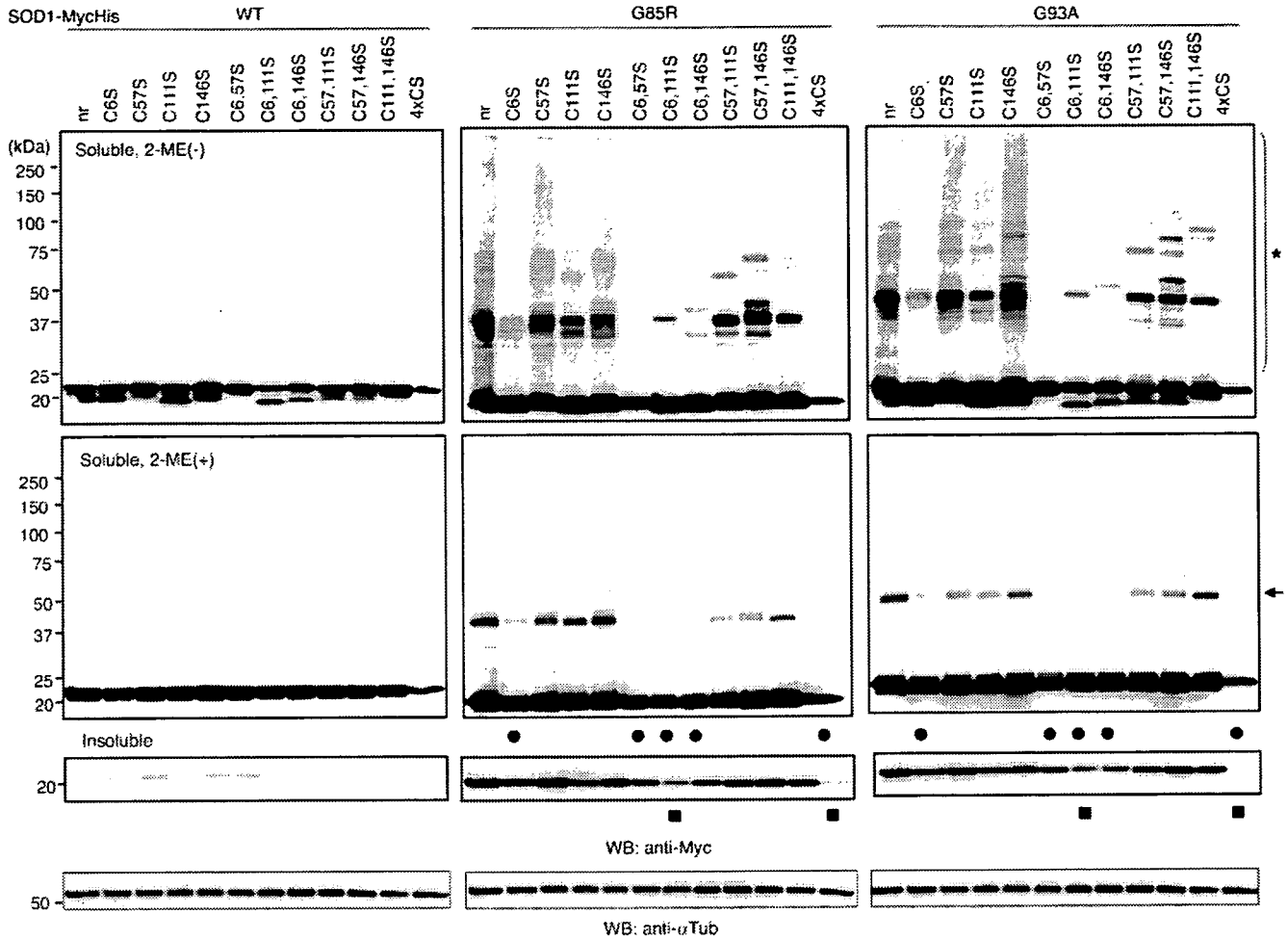

FIGURE 2. **Free Cys^6 and Cys^{111} are important for generating intermolecular disulfide-linked species and insoluble, sedimentable forms of mutant human SOD1.** Various combinations of replacing Cys with Ser were introduced into wild-type (*WT*) and mutant (G85R and G93A) SOD1-MycHis. Neuro-2a cells expressing SOD1-MycHis were treated with 2 μM MG132 for 24 h. Soluble fractions were analyzed by SDS-PAGE in the absence (*upper panels*) or presence (*middle panels*) of 2-ME. Insoluble fractions were analyzed by SDS-PAGE in the presence of 2-ME (*lower panels*). *Asterisk*, a disulfide-linked high molecular weight species; *arrow*, an SDS-resistant dimer of mutant SOD1. *Filled circles*, marked reduction of an SDS-resistant dimer with a Cys^6 replacement of mutant SOD1; *filled squares*, further reduction of the detergent-insoluble, sedimentable form of mutant SOD1 with simultaneous Cys^6 and Cys^{111} replacements. *nr*, SOD1 without replacement in cysteine residue; *4×CS*, all four cysteines replaced by serines.

amino acids changes by the anti-SOD1 antibody. Interestingly, none of the Cys residue replacements generated disulfide-linked species in wild-type SOD1 proteins (Fig. 2, *left panel*). Under reducing conditions, replacement of Cys^6 had a stronger effect on the formation of disulfide-linked species of mutant SOD1 than did the other three Cys residue replacements (Fig. 2, *middle* and *right panels, asterisk*). Combinations of replacing Cys^6 and one of the other Cys residues further attenuated the aberrant disulfide-linking of mutant SOD1 seen with the single substitution of Cys^6 (Fig. 2, *filled circle*). Under usual reducing conditions, the same reduced oligomerization of mutant SOD1 was observed when combinations of Cys^6 and other Cys residues were replaced (Fig. 2, *arrow*). The detergent-insoluble, sedimentable form of mutant SOD1 was also reduced especially if both Cys^6 and Cys^{111} were replaced (Fig. 2, *filled square*). Replacement of all four Cys residues completely abolished the disulfide-linked species in the non-reducing condition and the oligomeric, detergent-insoluble form of mutant SOD1 in the reducing condition (Fig. 2, *lane 4×CS*). Because simultaneous substitutions of Cys^6 and Cys^{111} had the strongest effects on the formation of aberrant species of mutant SOD1 in both non-reducing and reducing conditions, we compared C6S and C111S mutants with C57S and C146S mutants in the following experiments.

Substituting Both Cys^6 and Cys^{111} Greatly Reduces High Molecular Weight Aggregate Formation and Ubiquitylation of Mutant SOD1—In studies of polyglutamine disorders, it has been demonstrated that high molecular weight aggregates of mutant proteins are retained by filtration through cellulose acetate (25, 26). Cellulose acetate membranes usually bind protein very poorly and are used to trap high molecular weight structures from complex mixtures through filtration. This assay was also successfully applied to detect mutant SOD1 aggregation (27). Thus we used a cellulose acetate filter trap assay to investigate whether SOD1 proteins with Cys substitutions are retained in high molecular weight aggregates from lysates of SOD1-MycHis expressing Neuro-2a cells. Cells were lysed in TNE buffer, fractionated into crude denucleated, soluble, and insoluble fractions, and each fraction was then filtered through a 0.22-μm cellulose acetate membrane. Subsequent staining

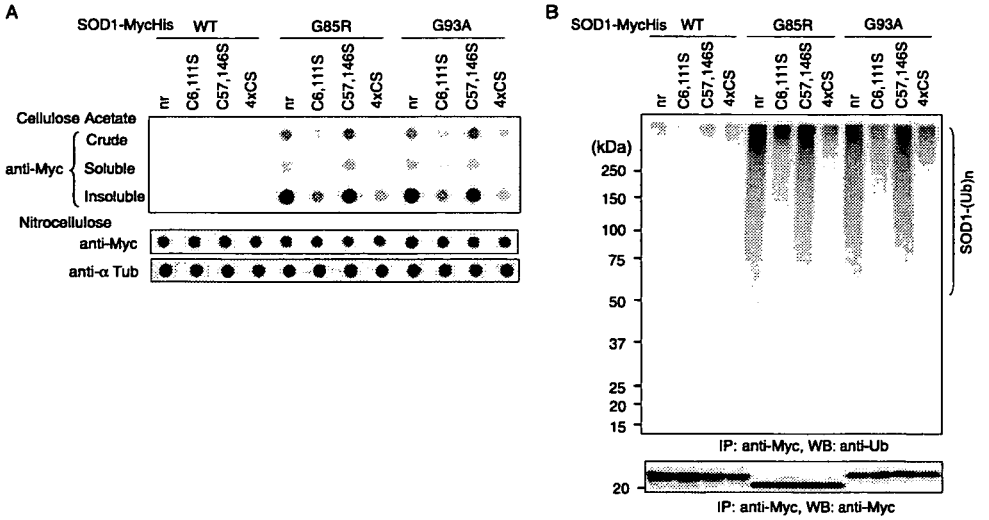

FIGURE 3. **Replacing both Cys^6 and Cys^{111} greatly reduces high molecular weight aggregate formation and ubiquitylation of mutant SOD1-MycHis.** *A*, crude, soluble, and insoluble fractions of cell lysates were analyzed by filter trap assay (*upper panel*). Nitrocellulose dot blots probed with anti-Myc (*middle panel*) and anti-α-tubulin (*lower panel*) antibodies were used as loading controls. *B*, *in vivo* ubiquitylation assay. Western blotting of SOD1-Myc-His immunoprecipitates with anti-ubiquitin antibody demonstrated polyubiquitylation of mutant SOD1s and their C57, 146S derivatives. Replacement of Cys^6 and Cys^{111} abolished polyubiquitylation of mutant SOD1. *nr*, SOD1 without replacement in cysteine residue; *4×CS*, all four cysteines replaced by serines.

with anti-Myc antibody revealed trapped SOD1 proteins (Fig. 3*A*, *upper panel*). Interestingly, high molecular weight aggregates were abundantly detected in mutant SOD1^{G85R}, SOD1^{G93A}, and their C57S and C146S derivatives. Replacements of Cys^6 and Cys^{111} greatly reduced high molecular weight structures of mutant SOD1. No high molecular weight aggregates were present in either wild-type SOD1 or their Cys-substituted mutants.

Mutant, but not wild-type, SOD1 is conjugated to a multiubiquitin chain and degraded at the proteasome (20, 28). To assess whether SOD1 proteins are ubiquitylated, we carried out an *in vivo* ubiquitylation analysis by expressing SOD1^{WT}, SOD1^{G85R}, SOD1^{G93A}, and their Cys to Ser mutants in Neuro-2a cells in the presence of the proteasome inhibitor MG132. When SOD1 was then immunoprecipitated, mutant SOD1s, but not wild-type SOD1, were polyubiquitylated (Fig. 3*B*, *lane 1*). Replacement of both Cys^6 and Cys^{111} abolished ubiquitylation of mutant SOD1, whereas replacement of Cys^{57} and Cys^{146} did not affect the ubiquitylation status of mutant SOD1 (Fig. 3*B*, *lane 2 versus lane 3*). Wild-type SOD1 and its Cys-replacement mutants were not ubiquitylated at all. Replacing only one of the four Cys residues attenuated neither the formation of high molecular weight species nor the ubiquitylation of mutant SOD1 (data not shown). Thus, the presence of both Cys^6 and Cys^{111} is important for high molecular weight aggregate formation and ubiquitylation of mutant SOD1. Disulfide bond formation at Cys^6 or Cys^{111} is critical step for ubiquitylation of mutant SOD1.

Formation of Disulfide-linked Species of Mutant SOD1 Strongly Correlates with Visible Aggregate Formation and Neurotoxicity—Expression of mutant, but not wild-type, SOD1 induces large perinuclear intracytoplasmic aggregates in differentiated Neuro-2a cells and reduces cellular viability (20). We analyzed the role of mutant SOD1 Cys residues in aggregate formation and neurotoxicity in Neuro-2a cells. Replacements of Cys^6 and Cys^{111} significantly reduced the percentage of mutant SOD1^{G85R} and SOD1^{G93A} cells with visible aggregates (Fig. 4*A*). To further demonstrate the extent of aggregate formation, we isolated SOD1 aggregates with a procedure according to Lee *et al.* (24). Differentiated Neuro-2a cells bearing SOD1-GFP aggregates were extracted with 1% Nonidet P-40 in the culture dish, and the Nonidet P-40-soluble proteins were gently removed. Under this condition, the soluble monomeric SOD1 was completely removed, and the aggregates remained in the culture dish due to their association with unknown structures (24). The remaining Nonidet P-40-insoluble portion was then scraped and centrifuged at 80 × *g*. After the centrifugation at 80 × *g* for 15 min, the pellet fraction was found to contain exclusively the large inclusion bodies. Replacements of Cys^6 and Cys^{111} markedly reduced the number of inclusion bodies in G93A mutant SOD1-GFP (Fig. 4*B*). Mutant SOD1^{G85R} and SOD1^{G93A}, but not wild-type SOD1, are toxic in differentiated Neuro-2a cells as previously described (20). However, replacement of the Cys^6 and Cys^{111} residues markedly reduced this neurotoxicity (Fig. 4*C*), which was not affected by replacing the Cys^{57} and Cys^{146} residues. There were no significant differences among the expression levels of all the constructs (Fig. 4*D*). Thus, changes in inclusion formation and toxicity are not due to differences in altered expression. These results provide evidence of direct links among intermolecular disulfide bonding, ubiquitylated complex formation, visible aggregate formation, and neurotoxicity.

Preferential Occurrence of Disulfide-cross-linked Mutant SOD1 in the Affected Lesions of ALS Model Mice—Although mutant SOD1 is expressed at similar levels in both neuronal and non-neuronal tissues, the aggregated and ubiquitylated forms are selectively found in the pathological lesions of patients and mutant SOD1-transgenic mice (29, 30). Thus, we next examined whether mutant SOD1 is aberrantly disulfide-linked in various tissues from symptomatic mutant SOD1 transgenic mice. Western blotting analysis, using anti-SOD1 antibody under reducing and non-reducing (omitting reducing agent 2-ME) conditions, demonstrated that the expression levels of mutant SOD1 were nearly the same in all tissues examined. Each of the tissues showed some of the disulfide-linked mutant SOD1species; however, in the brain stem and spinal cord, the areas predominantly affected in mutant SOD1-linked ALS, there was increased formation of intermolecular disulfide-linked species of mutant SOD1 (Fig. 5). Thus, intermolecular disulfide-linked

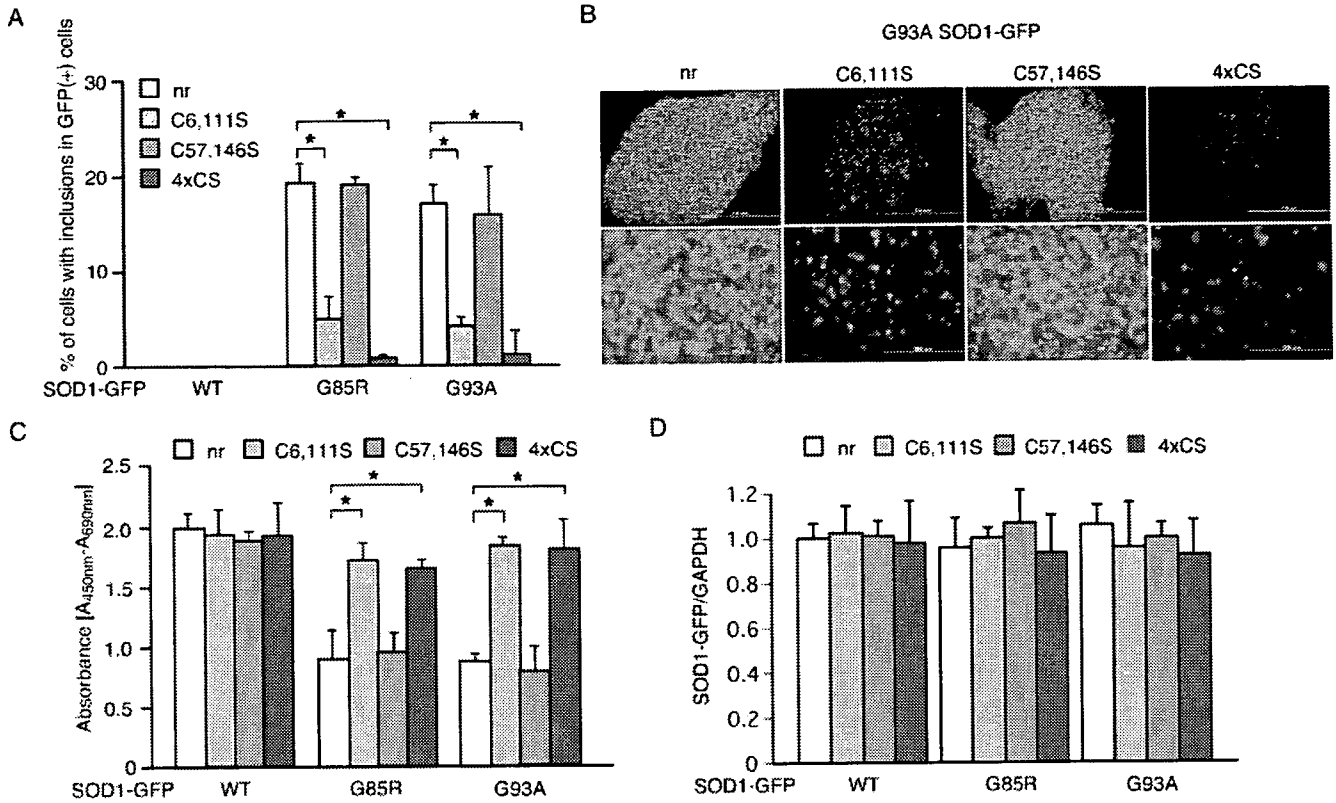

FIGURE 4. **Formation of disulfide-linked species of mutant SOD1 strongly correlates with visible aggregate formation and neurotoxicity.** *A*, the frequency of inclusion-bearing cells transfected with wild-type (*WT*), G85R, and G93A mutant SOD1-GFP and their Cys to Ser derivatives. *B*, G93A mutant SOD1-GFP inclusion bodies in 80 × *g* pellet. *Lower panels* are a high magnification image of the portion on the *upper panels* showing the whole pellet. The *scale bar* is equivalent to 10 mm in the *upper panels*, and 200 μm in the *lower panels*. *C*, change in the neurotoxic effect of mutant SOD1-GFP by Cys replacements to Ser. Cell viability was measured by the WST-1-based assay. *D*, all the constructs have equal expression. Transcription levels of SOD1-GFP in Neuro-2a cells expressing WT, G85R, and G93A mutant SOD1 and their Cys to Ser derivatives were examined by quantitative reverse transcription-PCR. Data were normalized with glyceraldehyde-3-phosphate dehydrogenase expression and then represent relative expression levels compared with levels in cells expressing WT SOD1-GFP. Data are mean ± S.D. values of triplicate assays. Statistical analyses were carried out by analysis of variance. *, $p < 0.01$. *nr*, SOD1 without replacing cysteine residues; *4×CS*, all four cysteines replaced by serines.

species are implicated as the aggregation-prone and neurotoxic intermediate of mutant SOD1 *in vivo*.

Effects of Cys^6- and Cys^{111}-mediated Disulfide Linking on the Rate of Mutant SOD1 Degradation—To determine whether replacement of Cys residues affects the degradation of SOD1 proteins, we examined the stability of mutant SOD1 proteins expressed in Neuro-2a cells (Fig. 6, *A* and *B*). Chase experiments with cycloheximide, which halts all cellular protein synthesis, demonstrated that replacement of Cys residues did not influence the stability of wild-type SOD1 protein (Fig. 6*A*). By contrast, although mutant SOD1 showed the enhanced degradation compared with wild-type proteins previously described (18–20), when both Cys^6 and Cys^{111} were replaced with Ser, the degradation of mutant SOD1 was markedly increased (Fig. 6*B*). Replacement of Cys^{57} and Cys^{146} did not significantly change the rate of degradation compared with Cys-native mutant SOD1 protein.

Ubiquityl Ligase Dorfin Ubiquitylates and Promotes Degradation of Disulfide-linked Mutant SOD1—We have previously shown that Dorfin physically binds and ubiquitylates various familial ALS-linked SOD1 mutants and enhances their degradation (20). Thus, we examined whether Cys residues on SOD1 affect the binding and ubiquitylating activities of Dorfin. To this end, Dorfin was co-expressed with wild-type or mutant SOD1 in Neuro-2a cells. Dorfin co-immunoprecipitated with G85R and G93A mutant SOD1s and their Cys^{57}- and Cys^{146}-replaced derivatives (Fig. 7*A*). However, Dorfin interacted with Cys^6- and Cys^{111}-replaced mutant SOD1 only very weakly and failed to bind to mutant SOD1 when all four Cys residues were replaced (Fig. 7*A*). Dorfin did not bind at all to wild-type SOD1. Using an *in vivo* ubiquitylation assay, we further examined whether co-expressed Dorfin enhances the ubiquitylation of Cys-substituted mutant SOD1 (Fig. 7*B*). When Cys-native or Cys^{57}- and Cys^{146}-replaced mutant SOD1s were co-expressed with Dorfin, ubiquitylation of mutant SOD1s were increased; however, co-expression of Dorfin with mutant SOD1 in which Cys^6 and Cys^{111} or all four Cys residues were replaced did not promote ubiquitylation of these mutant SOD1s (Fig. 7*B*). Chase experiments with cycloheximide in the presence or absence of Dorfin demonstrated that degradation of Cys-native and Cys^{57}- and Cys^{146}-replaced mutant SOD1^{G93A} was greatly accelerated when Dorfin was overexpressed, whereas the stability of Cys^6 and Cys^{111} or all four Cys-replaced mutant SOD1G93A were unaffected (Fig. 7*C*). We have previously shown that Dorfin exerts neuroprotective effects by promoting degradation of mutant SOD1 through its ubiquityl ligase activities (20). Co-expression of Dorfin improved the viability of Neuro-2a cells expressing Cys-

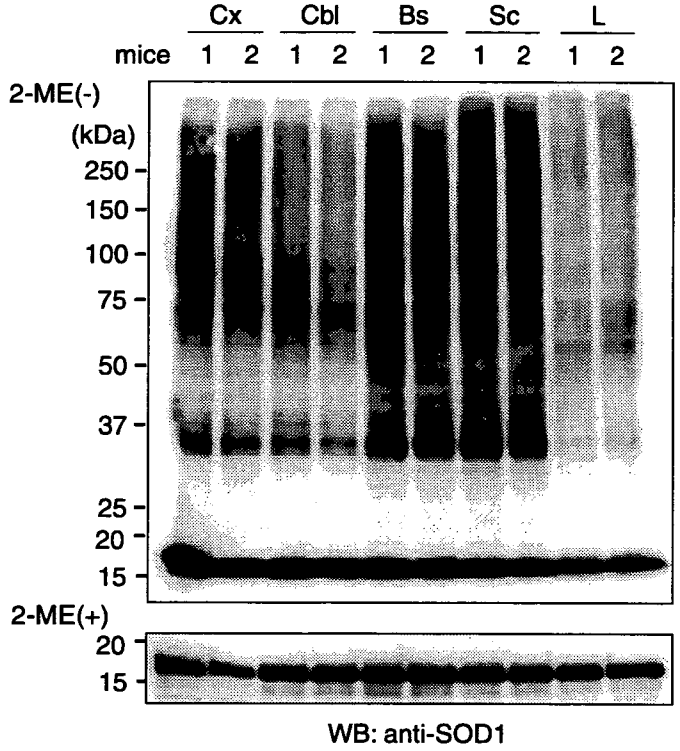

FIGURE 5. **Preferential occurrence of disulfide-cross-linked mutant SOD1 in the affected lesion of ALS model mice.** Western blotting of tissue samples from two 17-week-old symptomatic G93A mutant SOD1-transgenic mice under non-reducing (*upper panel*) and reducing (*lower panel*) conditions. *Cx*, cerebral cortex; *Cbl*, cerebellum; *Bs*, brain stem; *Sc*, spinal cord; *L*, liver.

native and Cys^{57}- and Cys^{146}-replaced mutant $SOD1^{G93A}$ (Fig. 7*D*).

DISCUSSION

Mutations in the *SOD1* gene cause familial ALS through the gain of a toxic function, however, the nature of this toxic function remains largely unknown (31). Ubiquitylated aggregates of mutant SOD1 proteins in affected lesions are a pathological hallmark of the disease (32) and suggest their relation to neurotoxicity. Recent biochemical studies suggest that the immature disulfide-reduced forms of the familial ALS mutant SOD1 proteins play a critical role in this neurotoxicity; *in vitro*, these forms tend to misfold, oligomerize, and readily undergo incorrect disulfide bond formation upon mild oxidative stress (16, 33). Among the more than 100 ALS-associated human SOD1 mutants, some cannot intrinsically form the essential intramolecular disulfide bonds. One of the conserved Cys residues, Cys^{146}, is missing in some of the mutants, such as the Leu^{126} del TT (stop at 131) and Gly^{127} ins TGGG (stop at 133); however, it has been reported that minute quantities of SOD1 aggregates can cause the disease in mice expressing the truncated mutant, Gly^{127} ins TGGG (stop at 133) (34). Furthermore, a significant fraction of the insoluble SOD1 aggregates in the spinal cord of ALS model mice contain multimers cross-linked via intermolecular disulfide bonds (17, 35). In the present study, we showed that non-physiological intermolecular disulfide bonds involving Cys^{6} and Cys^{111} of the mutant SOD1 were important for high molecular weight aggregate formation, ubiquitylation, and neurotoxicity *in vivo*, all of which were dramatically reduced in Neuro-2a cells when these residues were replaced with serines.

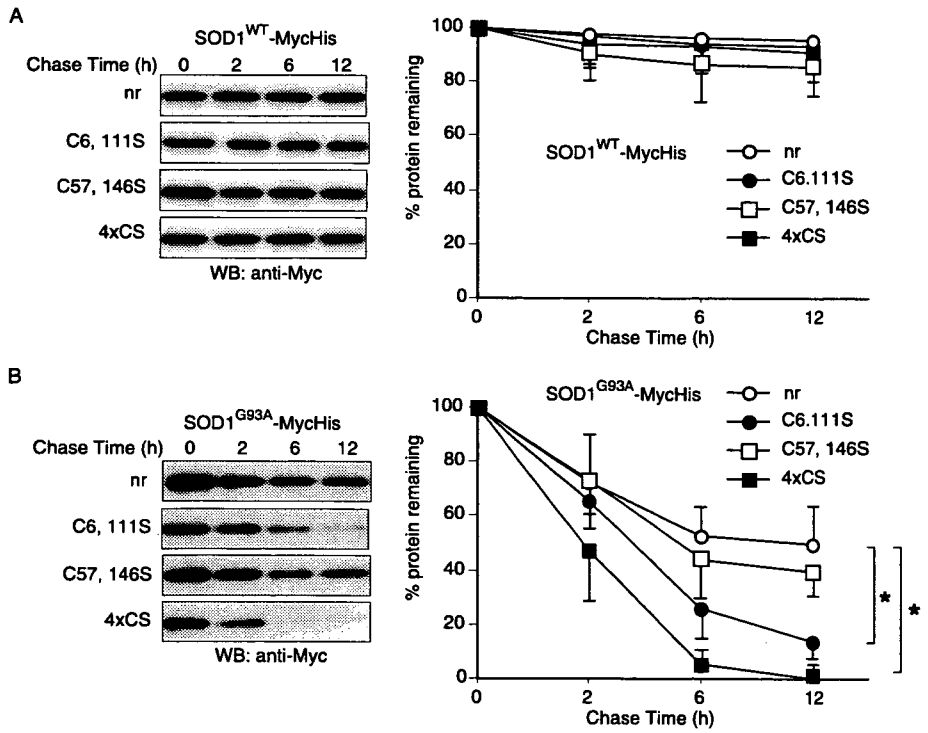

FIGURE 6. **Effects of disulfide-linking at Cys^{6} and Cys^{111} on the rate of mutant SOD1 degradation.** Cycloheximide chase analysis on Neuro-2a cells expressing (*A*) wild-type (*WT*) and (*B*) G93A mutant SOD1 and their Cys to Ser derivatives. Western blots showing levels of SOD1 protein at various times after the cycloheximide chase are in the *left panels*. Quantitative data on the right are mean ± S.D. values of three independent experiments. Statistical analyses were carried out by analysis of variance. *, $p < 0.01$. *nr*, SOD1 without cysteine residue replacement; *4×CS*, all four cysteines replaced by serines.

Human SOD1 has two free cysteine residues, Cys^{6} and Cys^{111} (36). Cys^{6} is located adjacent to the dimer interface pointed toward the interior of the β-barrel and is solute-inaccessible in the native, folded conformation. Cys^{111} is located near the surface and is solute-accessible and -reactive, often becoming blocked during purification (37). Replacement of the free Cys residues increased the resistance to thermal inactivation (38). Increased resistance of mutant SOD1s is due to increased resistance to irreversible unfolding and relatively unaffected by changes in conformational stability (39). Our data, showing that aggregate formation of mutant SOD1 is reduced when Cys^{6} and Cys^{111} are replaced with serines, are compatible with these observations. Mutations of the Cys^{6} residue (C6F and C6G) still result in familial ALS (4), and in a transgenic mouse expressing mouse SOD1 retaining cystines 6, 57, and 146 but lacking

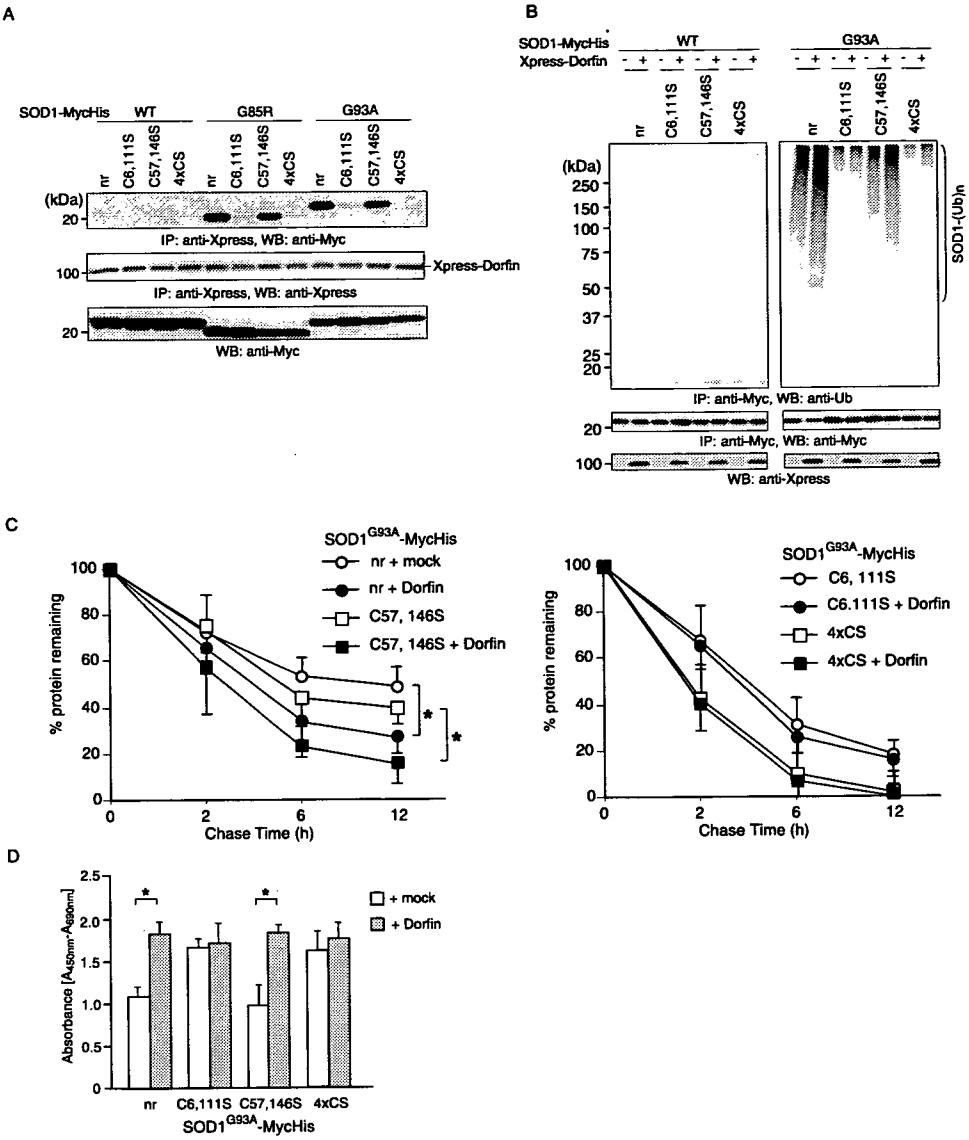

FIGURE 7. **Ubiquityl ligase Dorfin binds, ubiquitylates, and promotes degradation of disulfide-linked mutant SOD1.** *A*, replacement of Cys^6 and Cys^{111} nearly eliminated the interaction of Dorfin with mutant SOD1. Various SOD1-MycHis were co-transfected with Xpress-Dorfin. After immunoprecipitation with anti-Xpress antibody, the resulting precipitates and cell lysates were analyzed by Western blotting with anti-Myc antibody. *B, in vivo*, Dorfin failed to promote ubiquitylation of mutant SOD1 with the Cys^6 and Cys^{111} replacement. Western blotting of SOD1-Myc-His immunoprecipitates with anti-ubiquitin antibody. *C*, Dorfin failed to promote degradation of mutant SOD1 with both Cys^6 and Cys^{111} replaced. Cycloheximide chase analysis of G93A mutant SOD1 with Cys^6 and Cys^{111}-replacements (*left panel*) or with Cys^{57} and Cys^{146}-replacements (*right panel*) in the presence or absence of overexpressed Xpress-Dorfin. *D*, Dorfin prevented neurotoxicity by mutant SOD1 with intact Cys^6 and Cys^{111} residues. Cell viability was measured by the WST-1-based assay. Data are mean ± S.D. values of three independent experiments. Statistical analyses were carried out by unpaired *t* test. *, $p < 0.01$. *nr*, SOD1 without replacement in cysteine residue; *4×CS*, all four cysteines replaced by serines.

111 and with a G86R mutation corresponding to G85R mutation in human SOD1, degeneration of motor neurons in the spinal cord has been observed (40). These results imply that, if one of either the Cys^6 or Cys^{111} residues is present, it can still be a disease-causing SOD1. Our data here also revealed that replacement of only one of the Cys residues at positions 6 or 111 had modest effects on the formation of aggregates (Fig. 2).

Cytoplasmic proteins are degraded mainly via two pathways, the ubiquitin-proteasome pathway (6) and via autophagy (7). Previous studies have shown that mutant SOD1 proteins are turned over more rapidly than wild-type SOD1 (12, 18, 19). Two distinct ubiquitin ligases, Dorfin and NEDL1, were reported to specifically ubiquitylate mutant but not wild-type SOD1 (20, 21). These studies suggest that mutant SOD1 is degraded by the ubiquitin-proteasome pathway and that the accelerated turnover of mutant SOD1 is mediated in part by this pathway. Impairment of the proteasome activities may contribute to ALS pathogenesis (28, 41, 42). We showed here that proteasome inhibition led to a dose-dependent accumulation of aberrant disulfide-linked high molecular weight mutant SOD1 (Fig. 1), suggesting that disulfide-linking mediates ubiquitylation of mutant SOD1. In fact, we found that Dorfin ubiquitylated mutant SOD1 by recognizing the Cys^6 and Cys^{111} disulfide cross-linked form and targeted it for proteasomal degradation (Fig. 7). Mutant SOD1, in which the Cys^6 and Cys^{111} were replaced, was not ubiquitylated (Fig. 3), and its rate of degradation was not affected in the presence of Dorfin (Fig. 7). It is possible that mutant SOD1 lacking Cys^6 and Cys^{111} may be degraded directly by the proteasome without ubiquitylation (43) or by autophagy (44), but further studies are needed to address this issue.

The appearance of mutant SOD1 aggregates in motor neurons of familial ALS patients and mouse models has suggested that aggregation plays an important role in neurotoxicity (31). However, conflicting results have been reported on the correlation between aggregate formation and cell death. One report showed that aggregate formation of mutant $SOD1^{A4V}$ and $SOD1^{V148G}$ does not correlate with cell death (45), whereas another study using live cell-imaging techniques reported that the ability of mutant $SOD1^{G85R}$ and $SOD1^{G93A}$ proteins to form aggregates directly correlates with neuronal cell death (46). These controversies also exist in other neurodegenerative diseases (47, 48). In this study, we clearly showed a direct link among intermolecular disulfide bond-mediated high molecular weight complex formation, visible aggregate formation, and neurotoxicity (Figs. 2–4).

Furukawa *et al.* (16) reported that formation of disulfide-linked multimers need not involve the non-conserved Cys residues, Cys^6 and Cys^{111}, and that the conserved Cys residues, Cys^{57} and Cys^{146}, play an important role in the apo-form of

SOD1 multimerization upon oxidative stress. Our results underscore the importance of Cys^{6} and Cys^{111} for high molecular weight aggregate formation, ubiquitylation, and neurotoxicity in Neuro-2a cells. This discrepancy may result from differences in experimental conditions; we studied human SOD1 proteins expressed in Neuro-2a cells, and Furukawa *et al.* used the purified apo-form of human SOD1 from *Escherichia coli*. Further studies will clarify the roles of each of the Cys residues of the mutant SOD1 protein in the ALS pathogenesis *in vivo* by generating transgenic mice bearing mutant SOD1 lacking Cys^{6} and Cys^{111} or Cys^{57} and Cys^{146}.

REFERENCES

1. McCord, J. M., and Fridovich, I. (1969) *J. Biol. Chem.* **244,** 6049–6055
2. Fridovich, I. (1974) *Adv. Enzymol. Relat. Areas. Mol. Biol.* **41,** 35–97
3. Rosen, D. R. (1993) *Nature* **364,** 362
4. Valentine, J. S., Doucette, P. A., and Potter, S. Z. (2005) *Annu. Rev. Biochem.* **74,** 563–593
5. Crapo, J. D., Oury, T., Rabouille, C., Slot, J. W., and Chang, L. Y. (1992) *Proc. Natl. Acad. Sci. U. S. A.* **89,** 10405–10409
6. Fridovich, I. (1986) *Adv. Enzymol. Relat. Areas. Mol. Biol.* **58,** 61–97
7. Fisher, C. L., Cabelli, D. E., Tainer, J. A., Hallewell, R. A., and Getzoff, E. D. (1994) *Proteins* **19,** 24–34
8. Arnesano, F., Banci, L., Bertini, I., Martinelli, M., Furukawa, Y., and O'Halloran, T. V. (2004) *J. Biol. Chem.* **279,** 47998–48003
9. Freedman, R. B. (1995) *Curr. Opin. Struct. Biol.* **5,** 85–91
10. Lindenau, J., Noack, H., Possel, H., Asayama, K., and Wolf, G. (2000) *Glia* **29,** 25–34
11. Tiwari, A., and Hayward, L. J. (2003) *J. Biol. Chem.* **278,** 5984–5992
12. Borchelt, D. R., Lee, M. K., Slunt, H. S., Guarnieri, M., Xu, Z. S., Wong, P. C., Brown, R. H., Jr., Price, D. L., Sisodia, S. S., and Cleveland, D. W. (1994) *Proc. Natl. Acad. Sci. U. S. A.* **91,** 8292–8296
13. Ratovitski, T., Corson, L. B., Strain, J., Wong, P., Cleveland, D. W., Culotta, V. C., and Borchelt, D. R. (1999) *Hum. Mol. Genet* **8,** 1451–1460
14. Rakhit, R., Crow, J. P., Lepock, J. R., Kondejewski, L. H., Cashman, N. R., and Chakrabartty, A. (2004) *J. Biol. Chem.* **279,** 15499–15504
15. Doucette, P. A., Whitson, L. J., Cao, X., Schirf, V., Demeler, B., Valentine, J. S., Hansen, J. C., and Hart, P. J. (2004) *J. Biol. Chem.* **279,** 54558–54566
16. Furukawa, Y., and O'Halloran, T. V. (2005) *J. Biol. Chem.* **280,** 17266–17274
17. Furukawa, Y., Fu, R., Deng, H. X., Siddique, T., and O'Halloran, T. V. (2006) *Proc. Natl. Acad. Sci. U. S. A.* **103,** 7148–7153
18. Hoffman, E. K., Wilcox, H. M., Scott, R. W., and Siman, R. (1996) *J. Neurol. Sci.* **139,** 15–20
19. Johnston, J. A., Dalton, M. J., Gurney, M. E., and Kopito, R. R. (2000) *Proc. Natl. Acad. Sci. U. S. A.* **97,** 12571–12576
20. Niwa, J., Ishigaki, S., Hishikawa, N., Yamamoto, M., Doyu, M., Murata, S., Tanaka, K., Taniguchi, N., and Sobue, G. (2002) *J. Biol. Chem.* **277,** 36793–36798
21. Miyazaki, K., Fujita, T., Ozaki, T., Kato, C., Kurose, Y., Sakamoto, M., Kato, S., Goto, T., Itoyama, Y., Aoki, M., and Nakagawara, A. (2004) *J. Biol. Chem.* **279,** 11327–11335
22. Niwa, J., Ishigaki, S., Doyu, M., Suzuki, T., Tanaka, K., and Sobue, G. (2001) *Biochem. Biophys. Res. Commun.* **281,** 706–713
23. Marin, I., and Ferrus, A. (2002) *Mol. Biol. Evol.* **19,** 2039–2050
24. Lee, H. J., and Lee, S. J. (2002) *J. Biol. Chem.* **277,** 48976–48983
25. Scherzinger, E., Lurz, R., Turmaine, M., Mangiarini, L., Hollenbach, B., Hasenbank, R., Bates, G. P., Davies, S. W., Lehrach, H., and Wanker, E. E. (1997) *Cell* **90,** 549–558
26. Bailey, C. K., Andriola, I. F., Kampinga, H. H., and Merry, D. E. (2002) *Hum. Mol. Genet.* **11,** 515–523
27. Wang, J., Xu, G., and Borchelt, D. R. (2002) *Neurobiol. Dis.* **9,** 139–148
28. Urushitani, M., Kurisu, J., Tsukita, K., and Takahashi, R. (2002) *J. Neurochem.* **83,** 1030–1042
29. Gurney, M. E., Pu, H., Chiu, A. Y., Dal Canto, M. C., Polchow, C. Y., Alexander, D. D., Caliendo, J., Hentati, A., Kwon, Y. W., Deng, H. X., Chen, W., Zhai, P., Sufit, R. L., and Siddique, T. (1994) *Science* **264,** 1772–1775
30. Bruijn, L. I., Houseweart, M. K., Kato, S., Anderson, K. L., Anderson, S. D., Ohama, E., Reaume, A. G., Scott, R. W., and Cleveland, D. W. (1998) *Science* **281,** 1851–1854
31. Cleveland, D. W., and Rothstein, J. D. (2001) *Nat. Rev. Neurosci.* **2,** 806–819
32. Watanabe, M., Dykes-Hoberg, M., Culotta, V. C., Price, D. L., Wong, P. C., and Rothstein, J. D. (2001) *Neurobiol. Dis.* **8,** 933–941
33. Wang, J., Xu, G., and Borchelt, D. R. (2006) *J. Neurochem.* **96,** 1277–1288
34. Jonsson, P. A., Graffmo, K. S., Andersen, P. M., Brannstrom, T., Lindberg, M., Oliveberg, M., and Marklund, S. L. (2006) *Brain* **129,** 451–464
35. Deng, H. X., Shi, Y., Furukawa, Y., Zhai, H., Fu, R., Liu, E., Gorrie, G. H., Khan, M. S., Hung, W. Y., Bigio, E. H., Lukas, T., Dal Canto, M. C., O'Halloran, T. V., and Siddique, T. (2006) *Proc. Natl. Acad. Sci. U. S. A.* **103,** 7142–7147
36. Getzoff, E. D., Tainer, J. A., Stempien, M. M., Bell, G. I., and Hallewell, R. A. (1989) *Proteins* **5,** 322–336
37. Briggs, R. G., and Fee, J. A. (1978) *Biochim. Biophys. Acta* **537,** 86–99
38. McRee, D. E., Redford, S. M., Getzoff, E. D., Lepock, J. R., Hallewell, R. A., and Tainer, J. A. (1990) *J. Biol. Chem.* **265,** 14234–14241
39. Lepock, J. R., Frey, H. E., and Hallewell, R. A. (1990) *J. Biol. Chem.* **265,** 21612–21618
40. Ripps, M. E., Huntley, G. W., Hof, P. R., Morrison, J. H., and Gordon, J. W. (1995) *Proc. Natl. Acad. Sci. U. S. A.* **92,** 689–693
41. Kabashi, E., Agar, J. N., Taylor, D. M., Minotti, S., and Durham, H. D. (2004) *J. Neurochem.* **89,** 1325–1335
42. Cheroni, C., Peviani, M., Cascio, P., Debiasi, S., Monti, C., and Bendotti, C. (2005) *Neurobiol. Dis.* **18,** 509–522
43. Di Noto, L., Whitson, L. J., Cao, X., Hart, P. J., and Levine, R. L. (2005) *J. Biol. Chem.* **280,** 39907–39913
44. Kabuta, T., Suzuki, Y., and Wada, K. (2006) *J. Biol. Chem.* **281,** 30524–30533
45. Lee, J. P., Gerin, C., Bindokas, V. P., Miller, R., Ghadge, G., and Roos, R. P. (2002) *J. Neurochem.* **82,** 1229–1238
46. Matsumoto, G., Stojanovic, A., Holmberg, C. I., Kim, S., and Morimoto, R. I. (2005) *J. Cell Biol.* **171,** 75–85
47. Arrasate, M., Mitra, S., Schweitzer, E. S., Segal, M. R., and Finkbeiner, S. (2004) *Nature* **431,** 805–810
48. Saudou, F., Finkbeiner, S., Devys, D., and Greenberg, M. E. (1998) *Cell* **95,** 55–66

J Neuropathol Exp Neurol

Vol. 66, No. 11
November 2007
pp. 1037–1044

ORIGINAL ARTICLE

Intrathecal Delivery of Hepatocyte Growth Factor From Amyotrophic Lateral Sclerosis Onset Suppresses Disease Progression in Rat Amyotrophic Lateral Sclerosis Model

Aya Ishigaki, MD, PhD, Masashi Aoki, MD, PhD, Makiko Nagai, MD, PhD, Hitoshi Warita, MD, PhD, Shinsuke Kato, MD, PhD, Masako Kato, MD, PhD, Toshikazu Nakamura, PhD, Hiroshi Funakoshi, MD, PhD, and Yasuto Itoyama, MD, PhD

Abstract

Hepatocyte growth factor (HGF) is one of the most potent survival-promoting factors for motor neurons. We showed that introduction of the HGF gene into neurons of G93A transgenic mice attenuates motor neuron degeneration and increases the lifespan of these mice. Currently, treatment regimens using recombinant protein are closer to clinical application than gene therapy. To examine its protective effect on motor neurons and therapeutic potential we administered human recombinant HGF (hrHGF) by continuous intrathecal delivery to G93A transgenic rats at doses of 40 or 200 μg and 200 μg at 100 days of age (the age at which pathologic changes of the spinal cord appear, but animals show no clinical weakness) and at 115 days (onset of paralysis), respectively, for 4 weeks each. Intrathecal administration of hrHGF attenuates motor neuron degeneration and prolonged the duration of the disease by 63%, even with administration from the onset of paralysis. Our results indicated the therapeutic efficacy of continuous intrathecal administration of hrHGF in transgenic rats and should lead to the consideration for further clinical trials in amyotrophic lateral sclerosis using continuous intrathecal administration of hrHGF.

Key Words: Amyotrophic lateral sclerosis, Continuous intrathecal delivery, Hepatocyte growth factor, Neurodegeneration, Superoxide dismutase-1 (SOD1), Transgenic rat.

From the Department of Neurology (AI, MA, MN, HW, YI), Tohoku University Graduate School of Medicine, Sendai, Japan; Tohoku University Hospital ALS Center (AI, MA, HW, YI), Sendai, Japan; Department of Neuropathology (SK), Institute of Neurological Sciences, Faculty of Medicine Tottori University, Yonago, Japan; Division of Pathology (MK), Tottori University Hospital, Yonago, Japan; and Division of Molecular Regenerative Medicine (TN, HF), Department of Biochemistry and Molecular Biology, Osaka University Graduate School of Medicine, Osaka, Japan.

Send correspondence and reprint requests to: Masashi Aoki, MD, PhD, Department of Neurology, Tohoku University Graduate School of Medicine, 1-1 Seiryo-machi, Sendai 980-8574, Japan; E-mail: aokim@mail.tains.tohoku.ac.jp

This work was supported by a grant from the Ministry of Health, Labor, and Welfare, Japan (YI, MA, SK, HF). Research funding was also provided by the Haruki ALS Research Foundation (YI, MA, HW) and by a Grant-in-Aid for Scientific Research from the Ministry of Education, Culture, Sports, Science, and Technology, Japan (MA, SK, HF).

INTRODUCTION

Amyotrophic lateral sclerosis (ALS) is a fatal neurodegenerative disease caused by selective motor neuron death (1). Approximately 10% of cases of ALS are inherited, usually as an autosomal dominant trait (2). In ~25% of familial cases, the disease is caused by mutations in the gene encoding cytosolic copper-zinc superoxide dismutase (SOD1) (3–5). The cause of ALS is still unclear, and clinical trials have as yet failed to identify any truly effective therapeutic regimens for ALS, with only riluzole providing a modest improvement in survival. Various substances have been shown to have therapeutic effects in a murine model of ALS. However, there have been a few reports of prolongation of survival with treatment starting around the time of disease onset (6–12).

We (13) and another group (14) developed a rat model of ALS expressing a human SOD1 transgene with 2 ALS-associated mutations: glycine to alanine at position 93 (G93A) and histidine to arginine at position 46 (H46R) (3, 5). Similar to its murine counterpart, this rat transgenic (Tg) ALS model reproduces the major phenotypic features of human ALS. Some experimental manipulations are difficult in Tg mice because of size limitations; however, this Tg rat model allows routine implantation of infusion pumps for intrathecal drug delivery. Intrathecal drug application is a well-established method for therapy and has been used in clinical trials in patients with ALS (15). This route of administration bypasses the blood-brain barrier, allowing rapid access to potential binding sites for the test compound in the spinal cord (16).

Hepatocyte growth factor (HGF) was first identified as a potent mitogen for mature hepatocytes and was first cloned in 1989 (17). Detailed studies indicated that HGF is expressed in the CNS (18) and is a novel neurotrophic factor (19, 20). HGF is one of the most potent survival-promoting factors for motor neurons, comparable to glial cell line-derived neurotrophic factor in vitro (21). Sun et al (22) reported that introduction of the HGF gene into neurons of G93A Tg mice attenuates motor neuron degeneration and increases the lifespan of these mice. Thus, HGF is a good candidate agent for treatment of ALS. Currently, treatment using recombinant protein is closer to clinical application than gene therapy. However, HGF has a very

short half-life (23–25) and shows poor penetration into the CNS. Therefore, we examined the effects of continuous intrathecal delivery of human recombinant HGF (hrHGF) into Tg rats using implanted infusion pumps for selective and less invasive supply of HGF to the spinal cord.

MATERIALS AND METHODS

Animal Preparation and Clinical Evaluation

G93A Tg rats were genotyped by polymerase chain reaction (PCR) assay using DNA obtained from the tail as described (13). To examine the dose and effects of hrHGF on disease onset, we began administration of 40 or 200 μg of hrHGF (provided by H. Funakoshi and T. Nakamura, Osaka University, Osaka, Japan) or vehicle (0.1 M sulfoxide PBS) for 4 weeks to groups of eight 100-day-old Tg rats, when the pathologic changes of the spinal cord appeared, but the animals did not show weakness. All animals were killed at 130 days by deep anesthesia, and the spinal cords were examined. Because treatment of patients with ALS patients is initiated only after diagnosis based on clinical signs and symptoms, we tested the effects of hrHGF on survival with administration beginning at around the age of onset of paralysis. We administered 200 μg of hrHGF or vehicle alone to groups of eight 115-day-old G93A Tg rats for 4 weeks, and the animals were observed until their death. To analyze the mechanism of action of hrHGF administration beginning at onset of paralysis we treated groups of six 115-day-old G93A Tg rats with 100 μg of hrHGF or with vehicle alone for 2 weeks (a dose comparable to 200 μg for 4 weeks). All rats were killed 2 weeks after commencement of administration of hrHGF, and their lumbar spinal cords were examined. Further groups of 3 G93A Tg rats and 3 non-Tg rats at 70, 100, and 130 days were used to measure the levels of rat HGF and c-Met. All rats were handled according to approved animal protocols of our institution and had free access to food and water throughout the experimental period and before and after pump implantation.

The onset of ALS was scored as the first observation of abnormal gait, evidence of limb weakness, or loss of extension of the hindlimbs when picked up at the base of the tail. We defined the appearance of paralysis as disease onset, although this is not a sensitive indicator and appears later than the decrease in activity (10). However, the appearance of paralysis is a suitable marker of disease onset because it is closer to the state at which patients will be diagnosed with the disease.

Footprints were collected every 3 days by letting the rats walk on a straight path after dipping their hind paws in black ink. We measured 3 strides within the area showing regular gait and calculated the means. Footprint measurements were made for rats that began treatment at 115 days. Examiners were blinded to which group each of the rats belonged in.

Preparation of the Osmotic Pumps and Transplant Surgery

Osmotic pumps (model number 2004 or 2002; Durect Corporation, Cupertino, CA) were incubated in sterile saline at 37°C for 40 hours to attain a constant flow rate before use. Pumps were filled to capacity with hrHGF solution or vehicle using a filling needle. An infusion tube was made by connecting a 1-cm length of polyethylene tubing (PE 60; Becton Dickinson, Franklin Lakes, NJ) to a small caliber tube 9 cm in length (PE 10; Becton Dickinson) using an adhesive (ARON ALPHA; Konishi Co., Osaka, Japan). The end of the infusion tube was connected to the shorter end of the flow moderator, the longer end of which was inserted into the pump.

Surgery for placement of the pump and intrathecal administration was performed as follows. Tg rats were anesthetized using diethyl ether and 1% halothane in a mixture of 30% oxygen and 70% nitrous oxide. The skin over the third to fifth lumbar spinal process was incised and the paravertebral muscles were separated from the vertebral lamina with scissors. The fifth lumbar vertebra was laminectomized, and the dura mater was exposed for insertion of the infusion tube. Particular care was taken not

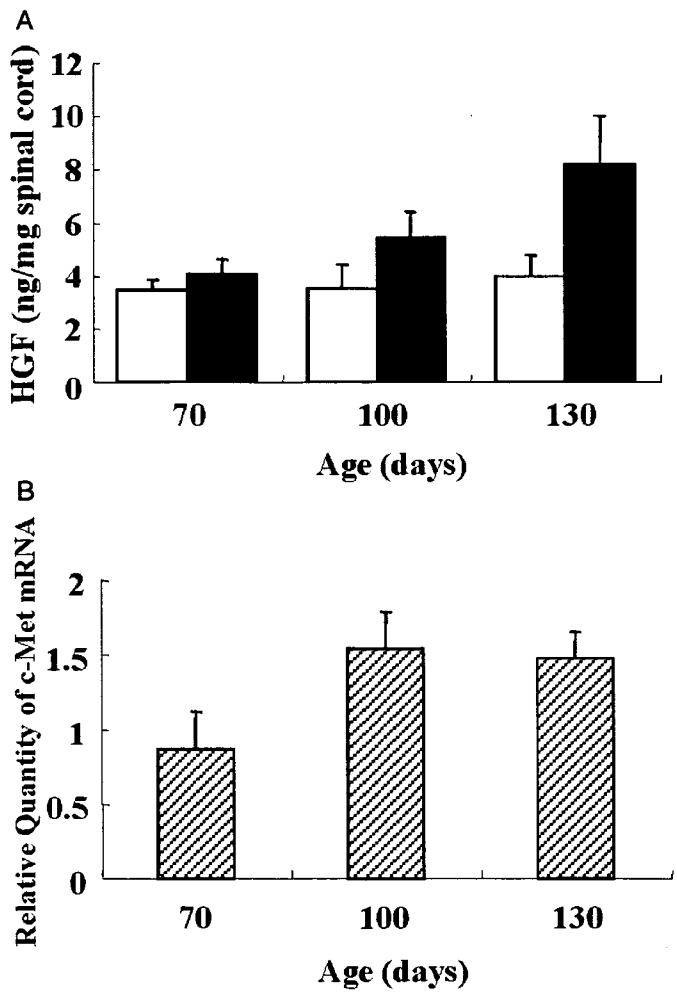

FIGURE 1. Increased levels of rat hepatocyte growth factor (HGF) and c-Met expression in the spinal cords of G93A transgenic (Tg) rats (n = 3) and non-Tg rats (n = 3). **(A)** Levels of endogenous rat HGF expression. Open bars, non-Tg rats; closed bars, G93A Tg rats. **(B)** Levels of c-Met mRNA of G93A Tg rats compared with non-Tg rats.

to injure the dura mater during laminectomy. A small hole was bored through the dura mater with a 24-gauge needle, and a polyethylene tube (PE 10, Becton Dickinson) was inserted into the subarachnoid space approximately 3 cm rostrally. A subcutaneous pocket was made into which the osmotic pump and pump side tube were implanted. The infusion tube was attached to the fascia over the paravertebral muscles at the incision margin with silk string. A drop of adhesive (ARON ALPHA) was applied, and the incision was closed by suturing the muscles and skin.

Measurement of Rat and Human HGF in the Lumbar Spinal Cord

Slices of the fifth lumbar cord from 3 G93A Tg rats and 3 non-Tg rats at 70, 100, and 130 days as well as from 130-day-old G93A Tg rats treated with 40 or 200 μg of hrHGF or vehicle alone for 4 weeks starting at 100 days were homogenized in buffer (20 mM Tris-HCl, pH 7.5, 0.1% Tween-80, 1 mM phenylmethylsulfonyl fluoride, and 1 mM EDTA) and centrifuged at 15,000 rpm for 30 minutes. Supernatants were separated and the concentrations of rat endogenous HGF were measured using an enzyme-linked immunosorbent assay (ELISA) kit, which is specific for rat HGF without detecting human HGF (22) (Institute of Immunology, Tokyo, Japan). For measurement of human HGF in the treated rats we used a human HGF-specific ELISA kit (IMMUNIS, Institute of Immunology), which is not reactive with rat HGF (26, 27).

Measurement of c-Met mRNA in the Lumbar Spinal Cord of Tg Rats

Aliquots of 1 μg of total RNA from the lumbar cords of rats were used as templates for synthesis of double-stranded cDNA. Real-time quantitative PCR was performed for c-Met and glyceraldehyde-3-phosphate dehydrogenase (GAPDH) [GAPDH forward primer, 5′-CCATCACTGCCACTCAGAAGAC-3′; GAPDH reverse primer, 5′-TCATACTTGGCAGGTTTCTCCA-3′; GAPDH TaqMan probe, 5′(FAM)-ACCACGAGCACTGTTTCAATAGGACCC-(TAMRA)3′; c-MET forward primer, 5′-GTACGGTGTCTCCAGCATTTTT-3′; c-Met reverse primer, 5′-AGAGCACCACCTGCATGAAG-3′; TaqMan probe, 5′(FAM)-CGTGTTCCTACCCCCAATGTATCCGT- (TAMRA)3′]. An ABI Prism 7700 Sequence Detection System (Applied Biosystems Perkin-Elmer, Foster City, CA) was used to monitor emission intensities using the above primer pairs and TaqMan fluorogenic probes. The c-Met mRNA level of G93A Tg rats relative to non-Tg rats was calculated using the Comparative C_T Method (Applied Biosystems).

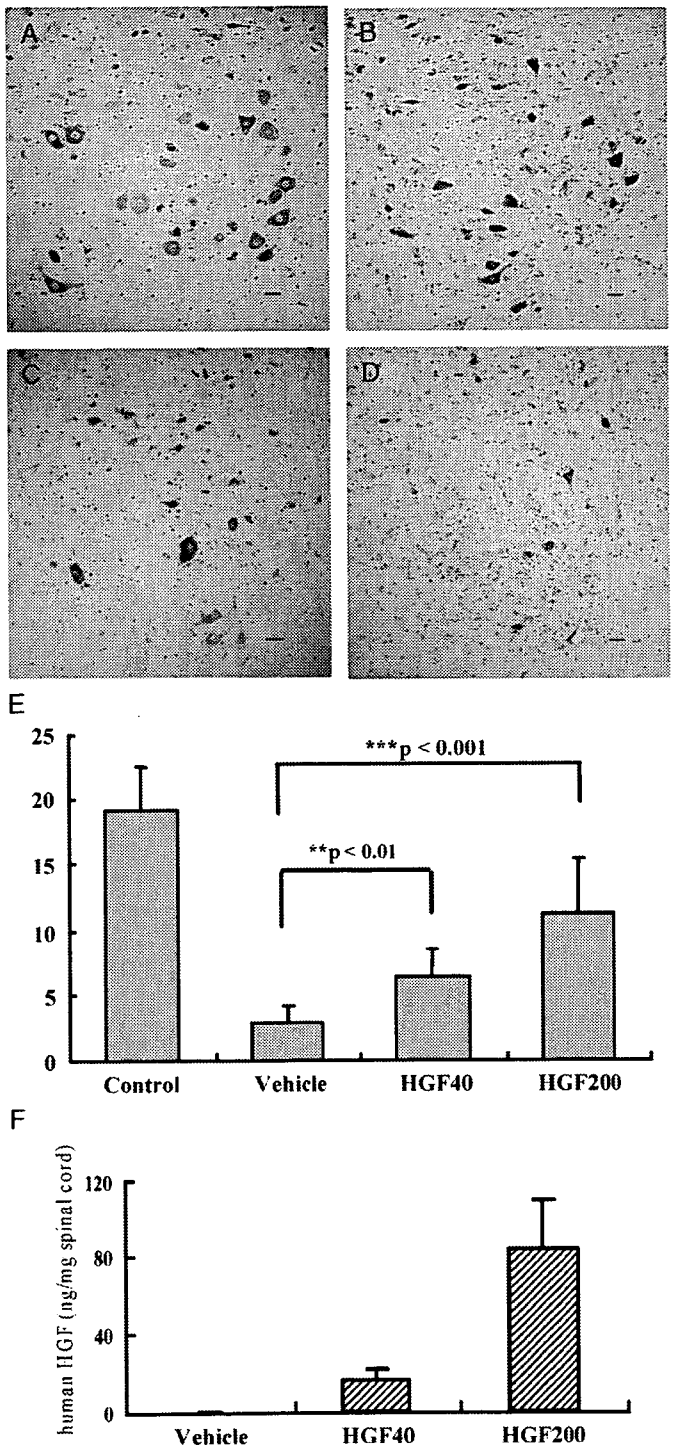

FIGURE 2. Intrathecal administration of hepatocyte growth factor (HGF) to G93A transgenic (Tg) rats at 100 days showed a protective effect against motor neuron death. **(A–D)** Histologic evaluation of the anterior horn with Nissl staining at 130 days: **(A)** lumbar cord of non-Tg rats; **(B)** 200 μg of human recombinant HGF (hrHGF)-treated; **(C)** 40 μg of hrHGF-treated; and **(D)** vehicle-treated G93A Tg rats. Scale bar = 40 μm. **(E)** Quantitative morphometric evaluation of surviving motor neurons of the fifth lumbar anterior horn at 130 days. We counted neurons that were >40 μm in diameter. Significantly larger numbers of motor neurons survived in hrHGF-treated G93A Tg rats ($p < 0.01$ and $p < 0.001$, 40 and 200 μg of hrHGF, respectively), compared with vehicle-treated G93A Tg rats (n = 8 in each group). **(F)** Levels of human HGF concentration in lumbar spinal cords of G93A Tg rats treated with 200 μg of hrHGF, 40 μg of hrHGF, and vehicle.

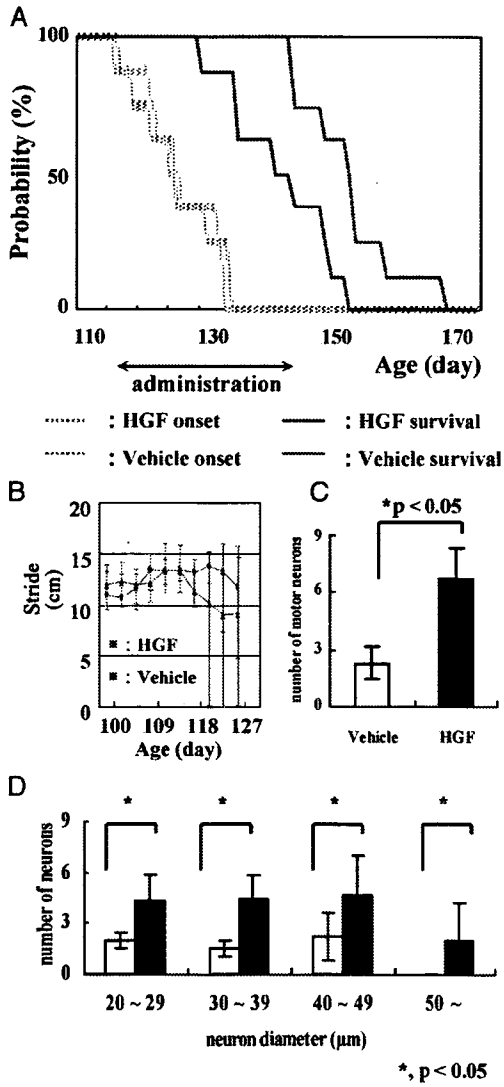

FIGURE 3. Intrathecal administration of hepatocyte growth factor (HGF) from 115 days (just before disease onset) retarded disease progression. **(A)** Survival periods were 143.25 ± 17.0 days in the vehicle-treated group (solid blue line) and 154.3 ± 16.4 days in the 200 μg of human recombinant HGF (hrHGF)-treated group (solid red line). Survival of hrHGF-treated animals was extended significantly ($p = 0.0135$), although there were no significant differences in onset (dotted lines, $n = 8$ in each group, $p = 0.6346$). **(B)** Footprint analysis demonstrated a delay in decline of stride length in G93A transgenic (Tg) rats treated with 200 μg of hrHGF relative to vehicle-treated G93A Tg rats (error bars, ± SD). **(C, D)** Quantitative morphometric evaluation of surviving motor neurons that were >40 μm in diameter **(C)** and neuron size distribution **(D)** in the fifth lumbar anterior horn of G93A Tg rats 2 weeks after administration from 115 days. Significantly larger number of motor neurons survived in the hrHGF-treated G93A Tg rats compared with vehicle-treated G93A Tg rats (6.7 ± 1.6 vs 2.3 ± 0.9; $p = 0.002$, $n = 6$ in each group) **(C)**.

Histopathologic and Immunohistochemical Analyses

To examine the dose and effects of hrHGF against disease onset, we began administration of 40 or 200 μg of hrHGF or vehicle alone to groups of eight 100-day-old Tg rats each for 4 weeks. At 130 days, G93A Tg rats were administered hrHGF or vehicle, and non-Tg rats were deeply anesthetized with diethyl ether and killed for histopathologic evaluation. To examine the effects of hrHGF administration beginning at onset of paralysis, 100 μg of HGF or vehicle alone was administered to groups of six 115-day-old Tg rats for 2 weeks. These animals were killed by deep anesthesia with diethyl ether 2 weeks after the operation. Under deep anesthesia these animals were perfused via the aorta with physiologic saline at 37°C and their lumbar spinal cords were removed. The fifth lumbar spinal cord tissue was embedded in OCT compound (Sakura Finetek Japan Co., Tokyo, Japan), frozen in an acetone/dry ice bath after fixation with 4% paraformaldehyde, and supplemented with 0.1 M cacodylate buffer (pH 7.3) containing 30% sucrose. Other spinal cord tissue specimens were frozen in dry ice and cut into frozen sections (12-μm-thick) and then washed with PBS. To evaluate the effects of HGF on motor neuron loss we compared the numbers of lumbar motor neurons in each group by counting as mentioned below. To evaluate the effects of HGF on apoptosis and to determine whether HGF receptors were activated, we compared the results of immunohistochemical staining of the lumbar cords for activated caspase-3, activated caspase-9 (Cell Signaling Technology, Inc., Beverly, MA), and phosphorylated c-Met (activated HGF receptor) (BioSource International, Camerillo, CA). The staining specificity of the antibodies was assessed by preabsorption of the primary antibody with excess peptide, omission of the primary antibody, or replacement of the primary antibody with normal rabbit IgG (22). We examined every seventh section from 42 serial sections of the fifth lumbar spinal cord. We counted neurons that had a clear nucleolus and were multipolar with neuronal morphology (13, 22), >40 μm in diameter, and located in a defined area of the anterior horn of the spinal cord. Cell counts were performed using ImageJ software (National Institutes of Health, Bethesda, MD) on images captured electronically (28).

Western Blotting

Lysates from the lumbar spinal cord of each rat were prepared in RIPA buffer (150 mM NaCl, 1% Nonidet P-40, 0.5% deoxycholate, 0.1% sodium dodecyl sulfate, and 50 mM Tris, pH 8.0). Equal amounts of proteins from the lysates (50 μg) were resolved by sodium dodecyl sulfate-polyacrylamide gel electrophoresis, transferred onto polyvinylidene diflouride membranes, and immunoblotted. The primary antibodies used were anti-caspase-3 (Sigma-Aldrich, St. Louis, MO), anti-caspase-9 (Stressgen Biotechnologies Corporation, Victoria, BC, Canada), anti-X-linked inhibitor of apoptosis protein (XIAP) (Cell Signaling Technology, Inc.), and anti-excitatory amino acid transporter 2 (EAAT2) antibodies (Chemicon International, Temecula, CA). After incubation of membranes with HRP-coupled

secondary antibodies, proteins were visualized using ECL or ECL Plus Western Blotting Detection Reagents (Amersham Biosciences Inc., Piscataway, NJ) and a Fluorochem image analyzer (LAS-3000 mini; Fuji Photo Film Co., Tokyo, Japan).

Statistical Analysis

The Kaplan-Meier and log-rank test were used for statistical analyses of differences in onset and survival between groups. For statistical analyses of differences in body weight, footprint, motor neuron cell count, and Western blotting we used analysis of variance and post hoc tests. The data are reported as means ± SD.

RESULTS

Measurement of the Levels of Rat HGF and c-Met Expression in Untreated Animals

Groups of 3 G93A Tg rats and non-Tg rats at 70, 100, and 130 days were used to measure the levels of rat HGF without any treatment. In the lumbar cords of untreated G93A Tg rats, the HGF concentrations increased with disease progression (Fig. 1A). At 70 days the level of rat HGF in the lumbar cords of G93A Tg rats was 4.05 ± 0.6 ng/mg and was the same as that of non-Tg rats. Increases of 35% and 107% were observed in the rat HGF level at 100 and 130 days, respectively, compared with non-Tg rats.

In addition, we measured the levels of c-Met mRNA in the lumbar spinal cords of Tg rats relative to non-Tg rats by real-time quantitative PCR. In the lumbar cords of G93A Tg rats the level of c-Met mRNA expression was the same as that in non-Tg rats at 70 days. However, a 55% increase in the level of c-Met mRNA expression compared with that of non-Tg rats was observed at 100 days and the higher level of expression was retained at 130 days (Fig. 1B).

Administration of hrHGF to 100-Day-Old G93A Tg Rats for 4 Weeks

To examine the efficacy of hrHGF on motor neurons in the spinal cords of Tg rats against onset of disease we administered 40 and 200 μg of hrHGF or vehicle alone to 100-day-old G93A Tg rats for 4 weeks (n = 8 in each group). Animals were killed at 130 days, and their lumbar spinal cords were examined. Because administration of hrHGF for more than 30 days may induce antibodies against hrHGF, we did not treat rats for longer than this period. We confirmed elevation of human HGF concentrations in the lumbar cords of hrHGF-treated rats using a specific sandwich immunoassay. The mean human HGF concentrations were 83.9 ± 25.1, 15.6 ± 5.4, and 0 ng/mg for rats treated with 200 μg of hrHGF, 40 μg of hrHGF, and vehicle, respectively (Fig. 2F). The endogenous rat HGF concentration is 4 to 5 ng/mg at this age (Fig. 1A). The human HGF concentration in the spinal cord of G93A Tg rats treated with 200 μg of hrHGF

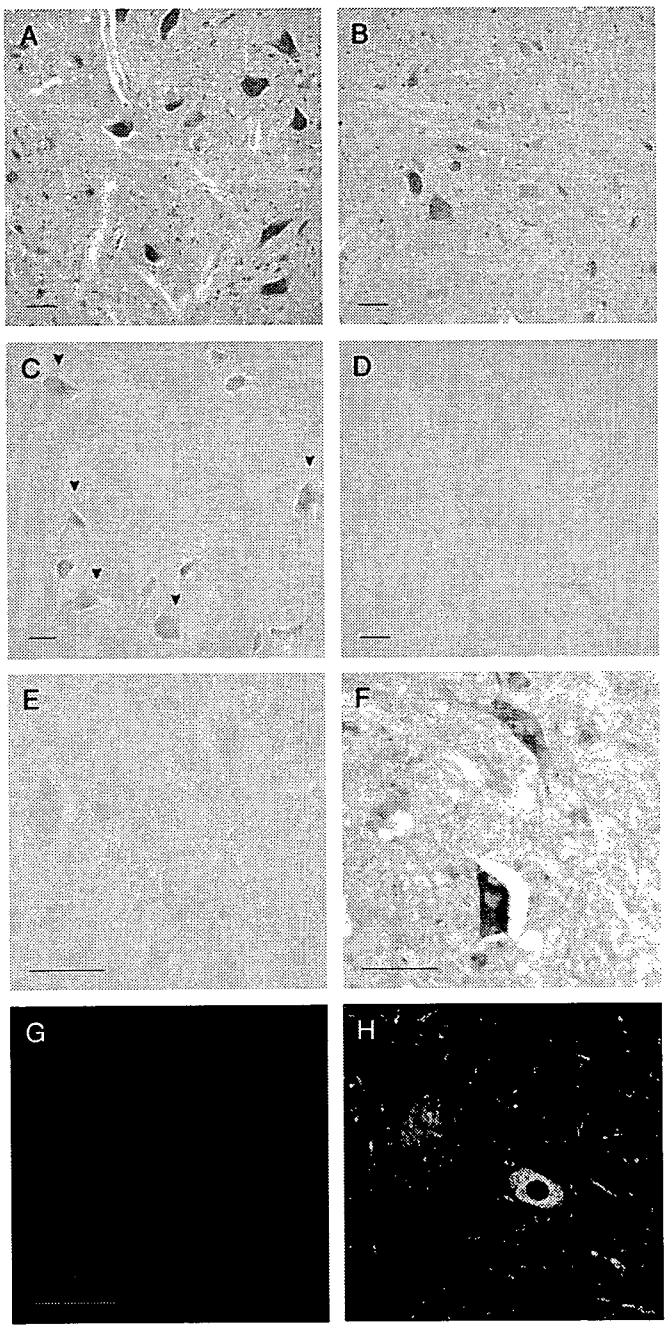

FIGURE 4. Sections of the fifth lumbar anterior horn from G93A transgenic (Tg) rats treated with human recombinant hepatocyte growth factor (hrHGF) **(A, C, E, G)** or vehicle **(B, D, F, H)** for 2 weeks starting at 115 days were stained with hematoxylin and eosin **(A, B)** and antibodies to phosphorylated c-Met **(C, D)**, activated caspase-3 **(E, F)**, and activated caspase-9 **(G, H)**. Scale bar = 50 μm. There were larger numbers of remaining large motor neurons in hrHGF-treated G93A Tg rats (6.7 ± 1.6) **(A)** than in vehicle-treated G93A Tg rats (2.3 ± 0.9) **(B)**. Phosphorylated c-Met staining was more distinct in hrHGF-treated G93A Tg rats **(C)** than in vehicle-treated G93A Tg rats **(D)**. In contrast, activated caspase-3 staining was stronger in vehicle-treated G93A Tg rats **(F)** than in hrHGF-treated G93A Tg rats **(E)**. Activated caspase-9 staining was detectable in vehicle-treated G93A Tg rats **(H)** compared with little reactivity in hrHGF-treated G93A Tg rats **(G)**.

was increased by approximately 20-fold relative to the endogenous rat HGF. All vehicle-treated G93A Tg rats developed weakness in the hindlimbs with a mean onset of 118.8 ± 4.3 days. Seven of 8 G93A Tg rats treated with 40 μg of rhHGF developed the disease before 130 days. In contrast, only 3 of 8 animals treated with 200 μg of rhHGF developed paralysis before this stage. At 130 days the average numbers of motor neurons in the ventral horn were as follows: non-Tg rats, 19.2 ± 3.3; vehicle only, 2.9 ± 1.3; 40 μg of hrHGF, 6.3 ± 2.1; and 200 μg of hrHGF, 11.2 ± 4.2. Significantly more motor neurons survived in hrHGF-treated (40 μg, $p < 0.01$; 200 μg, $p < 0.001$) than in vehicle-treated G93A Tg rats (Fig. 2A–E). hrHGF prevented motor neuron death in G93A Tg rats in a dose-dependent manner.

Administration of hrHGF to 115-Day-Old G93A Tg Rats for 4 Weeks

We next examined the therapeutic potential of HGF when administration was started at around the age of onset of paralysis. We administered 200 μg of hrHGF or vehicle alone to 115-day-old G93A Tg rats for 4 weeks. There were no statistically significant differences ($p = 0.6346$) in onset between the groups (200 μg of hrHGF, 126.8 ± 13.1 days; vehicle, 126.3 ± 13.8 days) (Fig. 3A, dotted lines). In contrast, 200 μg of hrHGF extended mean survival by 11 days compared with vehicle-treated G93A Tg rats ($p = 0.0135$) (Fig. 3A, solid lines), although G93A Tg rats showed very rapid disease progression and died within 20 days of disease onset. The average periods from the onset to death were 16.9 ± 8.17 and 27.5 ± 11.1 days in vehicle ($n = 8$) and hrHGF ($n = 8$) groups, respectively. The latter represented an increase of 62.7% relative to vehicle-treated controls. Footprint analysis of stride length in 200 μg of hrHGF-treated G93A Tg rats showed significant improvement compared with vehicle-treated G93A Tg rats at 118 days ($p = 0.0424$) (Fig. 3B). Thus, despite the very rapid disease progression in this model and short treatment period of 4 weeks, hrHGF treatment improved motor performance and prolonged survival even with treatment beginning around the onset of paralysis.

Histologic evaluation of the lumbar spinal cord indicated that hrHGF treatment prevented the pathologic changes typical of Tg rats. Two weeks after commencement of administration at 129 days, vehicle-treated rats showed substantial loss of motor neurons (2.3 ± 0.9) compared with hrHGF-treated rats (6.6 ± 1.6) (Figs. 3C, 4A, B). A significantly larger number of motor neurons survived in hrHGF-treated G93A Tg rats than in vehicle-treated G93A Tg rats ($p = 0.002$). Histologic evaluation of the lumbar spinal cord revealed much greater numbers of phosphorylated c-Met-positive cells (which were presumed to be motor neurons because of their large size, multipolar form, and localization in the anterior horn of the spinal cord) in hrHGF-treated G93A Tg rats compared with vehicle-treated G93A Tg rats at 2 weeks after the start of administration at 129 days (Fig. 4C, D). These observations indicated that the administered hrHGF was used in the spinal cord in G93A Tg rats. Consistent with the observation that apoptosis is involved in the pathogenesis of ALS (29–32), immunohistochemical analyses indicated large numbers of cells positive for activated caspase-3 and caspase-9 in vehicle-treated rats (Fig. 4F, H), compared with little or no reactivity in hrHGF-treated rats (Fig. 4E, G). To assess the mechanisms of suppression of caspase-3 and caspase-9 activation in hrHGF-treated rats, we next examined the level of XIAP by Western blotting, as XIAP inhibits activation of these procaspases and its levels are decreased in ALS mice (31). Western blotting analysis revealed increased XIAP expression

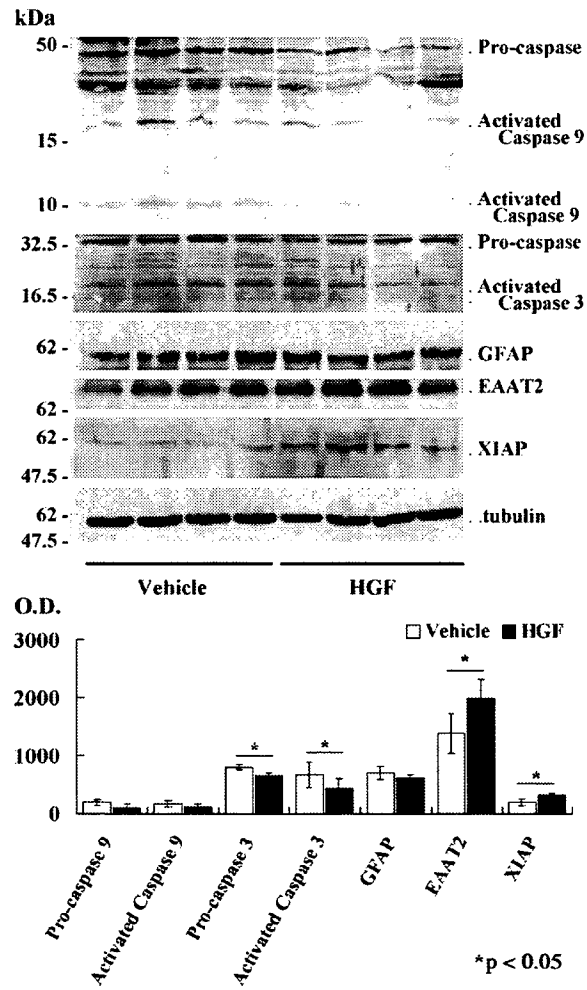

FIGURE 5. Caspase-3 and -9, glial fibrillary acidic protein (GFAP), excitatory amino acid transporter 2 (EAAT2), X-linked inhibitor of apoptosis protein (XIAP), and β-tubulin expression in the lumbar spinal cord. Western blotting of lumbar spinal cord lysates from G93A transgenic (Tg) rats treated with 100 μg of human recombinant hepatocyte growth factor (hrHGF) or vehicle for 2 weeks from 115 days. Western blotting analysis revealed increased levels of EAAT2 and XIAP expression in the spinal cords of hrHGF-treated G93A Tg rats compared with vehicle-treated G93A Tg rats (XIAP, $p = 0.0099$; EAAT2, $p = 0.0417$; $n = 4$). On the other hand, activated caspase-3 and -9 expression levels were decreased in hrHGF-treated G93A Tg rats. There were significant differences in caspase-3 expression between hrHGF- and vehicle-treated G93A Tg rats (pro-caspase-3, $p = 0.0031$; activated caspase-3, 0.0154; $n = 4$). GFAP expression was equivalent in both groups.

in the spinal cord of G93A Tg rats, and the increase in hrHGF-treated rats was only 60% of that in vehicle-treated G93A Tg rats. On the other hand, activated caspase-3 and 9 levels were decreased in hrHGF-treated G93A Tg rats ($p = 0.0154$ and $p = 0.2364$, 75% and 69% of vehicle-treated G93A Tg rats, respectively). These were all considered to be effects of HGF on motor neurons. Finally, we examined whether HGF improves the function of other cell types, such as astrocytes. There was a 60% increase in glial-specific glutamate transporter (EAAT2) in hrHGF-treated rats compared with vehicle-treated controls, although there was little difference in GFAP expression levels between the 2 groups (Fig. 5).

DISCUSSION

In this study, we demonstrated dose-dependent effects of hrHGF on motor neurons in the G93A Tg rat model of ALS, with administration starting at 100 days. Furthermore, we showed that hrHGF retards disease progression in this animal model treated from 115 days at the time of disease onset. There have been many studies of possible treatments in a mouse model of ALS (33, 34), but few agents have been shown to prolong survival with administration starting around disease onset (6–12). In this study, recombinant hrHGF retarded disease development even with administration beginning around the age onset of paralysis. Here, we showed the therapeutic effects of intrathecal delivery of a neurotrophic factor as a protein, rather than a transgene, on ALS beginning at the onset of paralysis. The average survival period of hrHGF-treated rats was 62.7% longer than that of vehicle-treated controls, comparable with the improved survival obtained by viral delivery of insulin-like growth factor-1 (6). We defined the appearance of paralysis as disease onset, although this is not a sensitive indicator and appears later than the decrease in activity (10). However, the appearance of paralysis is a clinically relevant marker of disease onset because it is closer to the state at which patients will be diagnosed with the disease.

We confirmed elevation of the human HGF concentration in the lumbar cords of hrHGF-treated G93A Tg rats using a specific sandwich immunoassay. Histologic evaluation of the lumbar spinal cord revealed greater numbers of phosphorylated c-Met-positive motor neurons in hrHGF-treated G93A Tg rats. This finding suggested that HGF receptors of motor neurons were activated well by administered hrHGF (35). These observations indicated that the administered hrHGF penetrated into the spinal cord and was utilized in the motor neurons of spinal cord. Previous studies demonstrated that many trophic factors have protective effects on motor neurons. In human trials of neurotrophic factors, such as brain-derived neurotrophic factors, glial cell line-derived neurotrophic factor, and insulin-like growth factor-1, the delivery (accessibility) of the protein to the motor neurons and glia in the spinal cord has been argued to be essential. Our results confirmed that chronic intrathecal administration with implanted infusion pumps supplied appropriate therapeutic doses to spinal cord motor neurons.

The HGF concentrations in cerebrospinal fluid are increased in many neurologic disorders, including ALS (26). In G93A Tg rats, the level of endogenous HGF in the spinal cord showed significantly greater elevation when the pathologic changes began in the spinal cord and increased with progression of the disease compared with the level of endogenous HGF in the spinal cord of non-Tg rats. After onset, the level of endogenous HGF almost doubled relative to that in non-Tg rats (Fig. 1A). These results were compatible to observations in patients with sporadic as well as familial ALS (36, 37). The level of c-met RNA expression in the lumbar cord of G93A rats increased to 155% of the normal level from before onset, and this elevated expression was retained after onset of disease (Fig. 1B). Kato et al (36) demonstrated that autocrine and paracrine trophic support of the HGF-c-met system contributes to attenuation of the degeneration of residual spinal cord motor neurons in ALS, whereas disruption of the HGF-c-met system at an advanced stage of disease accelerates cellular degeneration (37). Administration of hrHGF delayed the pathologic changes in G93A Tg rats. This effect of HGF may be due to replenishment of the relative insufficiency of HGF in G93A Tg rats in the present study.

Consistent with the findings that apoptosis is involved in ALS (29–31), large numbers of cells immunopositive for activated caspase-3 and -9 were observed in vehicle-treated animals in contrast to little or no reactivity in hrHGF-treated rats. This result was verified by quantitative Western blotting analysis, which indicated that HGF could block caspase activation of apoptosis. Caspase-3 and -9 are the main factors involved in execution of the caspase cascade. The survival-prolonging effect of HGF may be explained by suppression of induction and activation of caspase-9, as this enzyme is involved in determining disease duration (31). These observations suggest that the mechanism of the therapeutic effect of HGF in G93A Tg rats includes inhibition of the caspase cascade or of the cell death mechanism preceding the caspase cascade. In addition, EAAT2 and XIAP expression levels were increased in the hrHGF-treated group compared with vehicle-treated controls, indicating that HGF affected not only motor neurons via inhibition of the caspase cascade but also other cell types, such as astrocytes, which support motor neurons by maintaining or reinforcing internal cell protective functions, such as EAAT2 and XIAP.

Our results demonstrate pathologic improvements and retarded progression of ALS in G93A Tg rats by intrathecal administration of hrHGF from around the time of disease onset. Because HGF and c-Met are thought to be regulated in cases of not only familial but also sporadic ALS in a manner similar to the Tg mouse model of ALS (36), our findings suggest the possibility of clinical use of HGF in both familial and sporadic ALS. The results indicating the efficiency of hrHGF administration even from the onset of paralysis should prompt further clinical trials in ALS.

ACKNOWLEDGMENT

We thank Rieko Kamii for technical assistance.

REFERENCES

1. Rowland LP. Amyotrophic lateral sclerosis. Curr Opin Neurol 1994;7: 310–15
2. Mulder DW, Kurland LT, Offord KP, et al. Familial adult motor neuron disease: Amyotrophic lateral sclerosis. Neurology 1986;36:511–17

3. Rosen DR. Mutations in Cu/Zn superoxide dismutase gene are associated with familial amyotrophic lateral sclerosis. Nature 1993; 364:362
4. Deng HX, Hentati A, Tainer JA, et al. Amyotrophic lateral sclerosis and structural defects in Cu,Zn superoxide dismutase. Science 1993;261: 1047–51
5. Aoki M, Ogasawara M, Matsubara Y, et al. Mild ALS in Japan associated with novel SOD mutation. Nat Genet 1993;5:323–24
6. Kaspar BK, Llado J, Sherkat N, et al. Retrograde viral delivery of IGF-1 prolongs survival in a mouse ALS model. Science 2003;301:839–42
7. Azzouz M, Ralph GS, Storkebaum E, et al. VEGF delivery with retrogradely transported lentivector prolongs survival in a mouse ALS model. Nature 2004;429:413–17
8. Kieran D, Kalmar B, Dick JR, et al. Treatment with arimoclomol, a coinducer of heat shock proteins, delays disease progression in ALS mice. Nat Med 2004;10:402–5
9. Rothstein JD, Patel S, Regan MR, et al. β-Lactam antibiotics offer neuroprotection by increasing glutamate transporter expression. Nature 2005;433:73–77
10. Storkebaum E, Lambrechts D, Dewerchin M, et al. Treatment of motoneuron degeneration by intracerebroventricular delivery of VEGF in a rat model of ALS. Nat Neurosci 2005;8:85–92
11. Wu AS, Kiaei M, Aguirre N, et al. Iron porphyrin treatment extends survival in a transgenic animal model of amyotrophic lateral sclerosis. J Neurochem 2003;85:142–50
12. Crow JP, Calingasan NY, Chen J, et al. Manganese porphyrin given at symptom onset markedly extends survival of ALS mice. Ann Neurol 2005;58:258–65
13. Nagai M, Aoki M, Miyoshi I, et al. Rats expressing human cytosolic copper-zinc superoxide dismutase transgenes with amyotrophic lateral sclerosis: Associated mutations develop motor neuron disease. J Neurosci 2001;21:9246–54
14. Howland DS, Liu J, She Y, et al. Focal loss of the glutamate transporter EAAT2 in a transgenic rat model of SOD1 mutant-mediated amyotrophic lateral sclerosis (ALS). Proc Natl Acad Sci USA 2002;99: 1604–9
15. Ochs G, Penn RD, York M, et al. A phase I/II trial of recombinant methionyl human brain derived neurotrophic factor administered by intrathecal infusion to patients with amyotrophic lateral sclerosis Amyotroph Lateral Scler Other Motor Neuron Disord 2000;1:201–6
16. Ochs G, Giess R, Bendszus M, et al. Epi-arachnoidal drug deposit: A rare complication of intrathecal drug therapy. J Pain Symptom Manage 1999;18:229–32
17. Nakamura T, Nishizawa T, Hagiya M, et al. Molecular cloning and expression of human hepatocyte growth factor. Nature 1989;342: 440–43
18. Jung W, Castren E, Odenthal M, et al. Expression and functional interaction of hepatocyte growth factor-scatter factor and its receptor c-met in mammalian brain. J Cell Biol 1994;126:485–94
19. Matsumoto K, Nakamura T. HGF: Its organotrophic role and therapeutic potential. Ciba Found Symp 1997;212:198–211; discussion 11–14
20. Maina F, Klein R. Hepatocyte growth factor, a versatile signal for developing neurons. Nat Neurosci 1999;2:213–17
21. Ebens A, Brose K, Leonardo ED, et al. Hepatocyte growth factor/scatter factor is an axonal chemoattractant and a neurotrophic factor for spinal motor neurons. Neuron 1996;17:1157–72
22. Sun W, Funakoshi H, Nakamura T. Overexpression of HGF retards disease progression and prolongs life span in a transgenic mouse model of ALS J Neurosci 2002;22:6537–48
23. Liu KX, Kato Y, Narukawa M, et al. Importance of the liver in plasma clearance of hepatocyte growth factors in rats. Am J Physiol 1992;263: G642–49
24. Appasamy R, Tanabe M, Murase N, et al. Hepatocyte growth factor, blood clearance, organ uptake, and biliary excretion in normal and partially hepatectomized rats. Lab Invest 1993;68:270–76
25. Liu KX, Kato Y, Kino I, et al. Ligand-induced downregulation of receptor-mediated clearance of hepatocyte growth factor in rats. Am J Physiol 1998;275:E835–42
26. Funakoshi H, Nakamura T. Hepatocyte growth factor: From diagnosis to clinical applications. Clin Chim Acta 2003;327:1–23
27. Hayashi Y, Kawazoe Y, Sakamoto T, et al. Adenoviral gene transfer of hepatocyte growth factor prevents death of injured adult motoneurons after peripheral nerve avulsion. Brain Res 2006;1111:187–95
28. Grondard C, Biondi O, Armand AS, et al. Regular exercise prolongs survival in a type 2 spinal muscular atrophy model mouse. J Neurosci 2005;25:7615–22
29. Li M, Ona VO, Guegan C, et al. Functional role of caspase-1 and caspase-3 in an ALS transgenic mouse model. Science 2000;288: 335–39
30. Friedlander RM, Brown RH, Gagliardini V, et al. Inhibition of ICE slows ALS in mice. Nature 1997;388:31
31. Inoue H, Tsukita K, Iwasato T, et al. The crucial role of caspase-9 in the disease progression of a transgenic ALS mouse model. EMBO J 2003; 22:6665–74
32. Pasinelli P, Houseweart MK, Brown RH Jr. Caspase-1 and -3 are sequentially activated in motor neuron death in Cu,Zn superoxide dismutase-mediated familial amyotrophic lateral sclerosis. Proc Natl Acad Sci USA 2000;97:13901–6
33. Gurney ME, Pu H, Chiu AY, et al. Motor neuron degeneration in mice that express a human Cu,Zn superoxide dismutase mutation. Science 1994;264:1772–75
34. Gurney ME, Cutting FB, Zhai P, et al. Benefit of vitamin E, riluzole, and gabapentin in a transgenic model of familial amyotrophic lateral sclerosis. Ann Neurol 1996;39:147–57
35. Machide M, Hashigasako A, Matsumoto K, et al. Contact inhibition of hepatocyte growth regulated by functional association of the c-Met/ hepatocyte growth factor receptor and LAR protein-tyrosine phosphatase. J Biol Chem 2006;281:8765–72
36. Kato S, Funakoshi H, Nakamura T, et al. Expression of hepatocyte growth factor and c-Met in the anterior horn cells of the spinal cord in the patients with amyotrophic lateral sclerosis (ALS): Immunohistochemical studies on sporadic ALS and familial ALS with superoxide dismutase 1 gene mutation. Acta Neuropathol (Berl) 2003;106:112–20
37. Jiang YM, Yamamoto M, Kobayashi Y, et al. Gene expression profile of spinal motor neurons in sporadic amyotrophic lateral sclerosis. Ann Neurol 2005;57:236–51

An *In Vitro* Model for Lewy Body-Like Hyaline Inclusion/ Astrocytic Hyaline Inclusion: Induction by ER Stress with an ALS-Linked SOD1 Mutation

Satoru Yamagishi[1,2*☯¤a], Yoshihisa Koyama[1,2☯], Taiichi Katayama[1,2☯¤b], Manabu Taniguchi[1,2], Junichi Hitomi[1,2], Masaaki Kato[3], Masashi Aoki[3], Yasuto Itoyama[3], Shinsuke Kato[4*], Masaya Tohyama[1,2]

1 Department of Anatomy and Neuroscience, Graduate School of Medicine, Osaka University, Suita, Osaka, Japan, 2 The 21st Century Center of Excellence Program, Graduate School of Medicine, Osaka University, Suita, Osaka, Japan, 3 Department of Neurology, Tohoku University School of Medicine, Sendai, Japan, 4 Department of Neuropathology, Institute of Neurological Sciences, Faculty of Medicine, Tottori University, Yonago, Japan

Neuronal Lewy body-like hyaline inclusions (LBHI) and astrocytic hyaline inclusions (Ast-HI) containing mutant Cu/Zn superoxide dismutase 1 (SOD1) are morphological hallmarks of familial amyotrophic lateral sclerosis (FALS) associated with mutant SOD1. However, the mechanisms by which mutant SOD1 contributes to formation of LBHI/Ast-HI in FALS remain poorly defined. Here, we report induction of LBHI/Ast-HI-like hyaline inclusions (LHIs) *in vitro* by ER stress in neuroblastoma cells. These LHI closely resemble LBHI/Ast-HI in patients with SOD1-linked FALS. LHI and LBHI/Ast-HI share the following features: 1) eosinophilic staining with a pale core, 2) SOD1, ubiquitin and ER resident protein (KDEL) positivity and 3) the presence of approximately 15–25 nm granule-coated fibrils, which are morphological hallmark of mutant SOD1-linked FALS. Moreover, in spinal cord neurons of L84V SOD1 transgenic mice at presymptomatic stage, we observed aberrant aggregation of ER and numerous free ribosomes associated with abnormal inclusion-like structures, presumably early stage neuronal LBHI. We conclude that the LBHI/Ast-HI seen in human patients with mutant SOD1-linked FALS may arise from ER dysfunction.

Citation: Yamagishi S, Koyama Y, Katayama T, Taniguchi M, Hitomi J, et al (2007) An *In Vitro* Model for Lewy Body-Like Hyaline Inclusion/Astrocytic Hyaline Inclusion: Induction by ER Stress with an ALS-Linked SOD1 Mutation. PLoS ONE 2(10): e1030. doi:10.1371/journal.pone.0001030

INTRODUCTION

Amyotrophic lateral sclerosis (ALS) is a progressive neurodegenerative disorder in which both upper and lower motor neurons begin to degenerate in middle-aged persons. About 10% of ALS patients demonstrate autosomal dominant inheritance of this disease, a disorder known as familial ALS (FALS) [1–6]. About 20% of FALS cases are associated with mutations of the Cu/Zn-superoxide dismutase (SOD1) gene [7]. SOD1 is an abundant protein of approximately 153 amino acids that accounts for approximately 1% of total cytosolic protein. More than 100 different SOD1 mutations have been reported as risk factors in association with FALS.

The endoplasmic reticulum (ER) is responsible for the synthesis, initial post-translational modification, and proper folding of proteins, as well as for their sorting export and delivery to appropriate cellular destinations. A variety of conditions, such as loss of the intraluminal oxidative environment or loss of calcium homeostasis, can cause accumulation of misfolded proteins in the ER. To cope with such accumulation, there are three possible responses in eukaryotes. The first response is known as the unfolded protein response (UPR), in which IRE1α and ATF6 recognize aberrant proteins and increase the expression of ER-resident chaperones such as GRP78/BiP and GRP94 to promote proper protein folding [8,9]. The second response involves suppression of translation mediated by the serine/threonine kinase PERK, which phosphorylates and inactivates the translation initiation factor eIF-2α to reduce the production of misfolded proteins [10,11]. The third response is ER-associated degradation (ERAD), in which misfolded proteins are expelled from the ER and targeted for degradation by cytoplasmic proteasomes [12,13]. Although these three protective responses can transiently control the accumulation of misfolded proteins within the ER, they can be overcome by sustained 'ER stress' [14–16]. 'ER stress' is involved in neuronal death and various neurodegenerative disorders, such as Charcot-Marie-Tooth disease, and is especially related to inclusion body diseases such as Alzheimer's disease, Parkinson's disease, Huntington's disease and ALS [17–23].

Histopathologic studies have revealed that neuronal Lewy body-like hyaline inclusions (LBHI) and astrocytic hyaline inclusions (Ast-HI), are morphological hallmarks of mutant SOD1-linked FALS [24]. Neuronal LBHI and Ast-HI are ultrastructually identical and share various features, with both consisting of 15–25 nm granule-coated fibrils, both showing immunoreactivity for

Academic Editor: Xiao-Jiang Li, Emory University, United States of America

Received February 28, 2007; **Accepted** September 23, 2007; **Published** October 10, 2007

Funding: This work was supported in part by a grant from the 21st Century COE Program, Japan Society for the Promotion of Science, 6 Ichibancho, Chiyoda-ku, Tokyo 102-8471, Japan, a Grant-in-Aid for Scientific Research (c) from the Ministry of Education, Culture, Sports, Science and Technology of Japan (S.K.: 17500229), a Grant from Research on Psychiatric and Neurological Disease and Mental Health (SK, MA, YI) and a Research Grant on Measures for Intractable Diseases from the Ministry of Health, Labour and Welfare of Japan (SK, YI). SY is supported by a long-term fellowship by European Molecular Biology Organization (EMBO) and Japan Society for the Promotion of Science (JSPS).

Competing Interests: The authors have declared that no competing interests exist.

* **To whom correspondence should be addressed.** E-mail: yamagishi@neuro.mpg.de (SY); kato@grape.med.tottori-u.ac.jp (SK)

☯ These authors contributed equally to this work.

¤a **Current address:** Molecular Neurobiology, Max-Planck-Institute of Neurobiology, Martinsried, Munich, Germany,

¤b **Current address:** Department of Anatomy and Neuroscience, Hamamatsu University School of Medicine, Hamamatsu, Shizuoka, Japan

SOD1, ubiquitin, and copper chaperone for SOD (CCS), and both appearing late in the course of the disease (i.e. at ~10 to 30 years of age in humans [24–27]). Recently, Wate et al. reported that neuronal LBHI are immunoreactive for GRP78/BiP, a component of the UPR cellular response to ER stress [28].

In the present study, we show that ER stress in a neuroblastoma line expressing mutant SOD1 can provoke SOD1 aggregation in ER and formation of LBHI/Ast-HI-like hyaline inclusion bodies (LHIs), which show SOD1, ubiquitin, GRP78/BiP and ER resident protein (KDEL) immunopositivity similar to the shared cytopathological features of LBHI and Ast-HI. Induced neuroblastoma LHI furthermore consisted of 15–25 nm granule-coated fibrils, a hallmark of mutant SOD1-linked FALS, raising the possibility that these acutely induced aggregations represent a precursor to LBHI/Ast-HI seen in advanced FALS. In support of this possibility, we observe abnormal ER and numerous free ribosomes aggregated in the peri-nuclear region neuroblastoma cells expressing L84V SOD1 under ER stress condition and in spinal cord neurons in presymptomatic transgenic mice expressing L84V SOD1. Taken together, these findings suggest a model for early events in FALS cellular pathology, in which ER stress promotes the aggregation of mutant SOD1 and is involved in the development of LBHI/Ast-HI in patients with mutant SOD1 linked FALS.

RESULT

Aggregation and ubiquitination of mutant SOD1 under ER stress

To identify conditions which lead to the aggregation of mutant SOD1, we generated SK-N-SH human neuroblastoma cell lines that stably expressed FLAG-tagged human SOD1 encoding a leucine to valine substitution mutation (L84V) associated with FALS [29]. Western blot analysis confirmed that expression of endogenous and exogenous SOD1 was equal in the cell line (Fig. 1A). Reports that neuronal LBHI contain GRP78/BiP, an ER resident component of the UPR response, suggested that ER stress might be a factor in the aggregation of mutant SOD1 [28]. We therefore examined localization of wild-type and mutant SOD1 under normal conditions and under conditions of ER stress (Figure 1). Under normal conditions, wild-type and L84V SOD1 were distributed through the cytosol (Fig. 1B and D). However, following treatment with tunicamycin, an inhibitor of N-glycosylation which causes ER stress, small SOD1-positive aggregates (up to 3 μm in diameter) were seen in L84V SOD1-expressing cells (22.3%, $p<0.001$; Fig. 1E and F). A much smaller percentage of wild-type SOD1 expressing cells (2.9%, n.s.) showed non-inducible SOD1 aggregation (Fig. 1C and F). To confirm whether ER stress is required for the aggregation of SOD1, we compared tunicamycin and thapsigargin as ER stress inducers with etoposide as a non-ER stress inducer (causing DNA damage). Exposure to 1 and 3 μg/ml tunicamycin (21.1% and 17.5%, respectively) or 0.3 and 1 μM thapsigargin (27.0% and 27.2%, respectively) significantly increased the number of cells containing SOD1 aggregates, in L84V SOD1 expressing neuroblastoma cells. Treatment with 100 and 300 μM etoposide did not lead to a significant increase in aggregates (Fig. 1G). Thus mutant SOD1 forms aggregates following treatments provoking ER stress, but not following treatment causing damage to the nucleus.

Since the SOD1-positive inclusions of FALS patients are known to be eosinophilic [26], we performed hematoxylin-eosin (HE) and anti-SOD1 antibody staining to determine whether the aggregates induced in the neuroblastoma line were also eosinophilic.

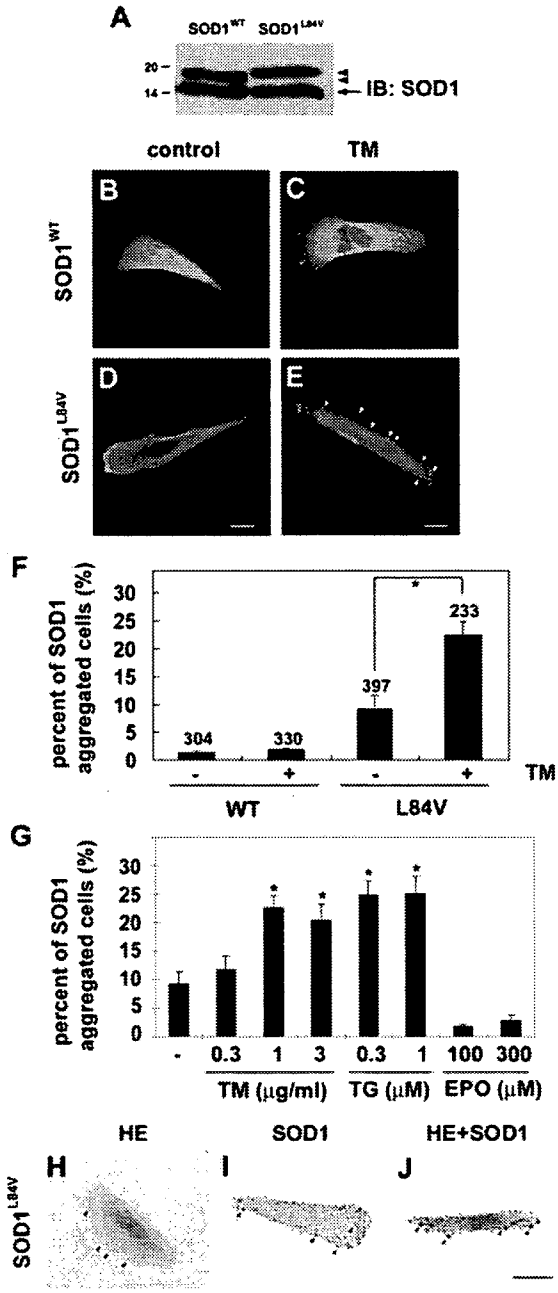

Figure 1. Eosinophilic aggregates of L84V SOD1 are induced by ER stress. (A) Western blotting analysis of the expression of SOD1 in SK-N-SH cells, which stably expressed FLAG tagged wild-type SOD1 or L84V mutant SOD1. Arrowheads and arrow indicate exogenous and endogenous SOD1, respectively. (B–D) Immunofluorescent analysis of SOD1 aggregates in SK-N-SH cells expressing wild-type SOD1 (B, C) or L84V SOD1 (D, E). Cells were incubated under control conditions (B, D) or with 1 μg/ml tunicamycin (C, E) for 24 h, and then were fixed and stained with an anti-SOD1 antibody. Tunicamycin induced aggregates of SOD1 (arrowheads) in L84V SOD1-expressing cells, but not in wild-type SOD1-expressing cells. Scale bar = 20 μm. (F) Quantification of (B-D). After the staining the cells with SOD1 aggregates were counted and scored. Numbers indicate the amounts of total counted cells. Asterisks show a significant difference from control, *$p<0.001$. (G) SOD1 aggregates induced by tunicamycin and thapsigargin, but not by etoposide. SK-N-SH cells expressing L84V SOD1 were exposed to 0.3, 1 and 3 μg/ml tunicamycin, 0.3 and 1 μM thapsigargin and 100 and 300 μM etoposide. Asterisks show a significant difference from control, *$p<0.001$. (H-J) Eosinophilic SOD1 aggregates induced by tunicamycin. Cells were treated as described in (E) and then stained with HE (H), anti-SOD1 antibody (I), or both (J). Scale bar = 20 μm.
doi:10.1371/journal.pone.0001030.g001

Figures 1H–J show that the aggregates induced by tunicamycin treatment were positive for both eosin and SOD1.

In patients with mutant SOD1-linked FALS, SOD1-positive aggregates are reported to be ubiquitinated by RING finger-type E3 ubiquitin ligases such as dorfin [30–33]. To investigate whether the SOD1 aggregates induced by ER stress were ubiquitinated, we performed double immunostaining with anti-SOD1 and anti-ubiquitin antibodies (Fig. 2 A–R). After treatment with either tunicamycin or ALLN, a specific proteasome inhibitor, wild-type and L84V SOD1-expressing cells were immunostained with anti-SOD1 and anti-ubiquitin antibodies. As a result, mutant SOD1 aggregates induced by either tunicamycin or ALLN were clearly colocalized with ubiquitin, suggesting the SOD1 were ubiquitinated. To further examine the ubiquitination of the mutant SOD1, a co-immunoprecipitation assay utilizing ubiquitin was performed (Fig. 2S). As expected, L84V SOD1-expressing cells showed a positive ubiquitin ladder after ALLN treatment, but wild-type SOD1-expressing cells did not.

Aggregates of SOD1 show positive localization to the ER, but not to the mitochondria, lysosomes, or Golgi apparatus

Under normal conditions, SOD1 is diffusely distributed throughout the cytoplasm. In contrast, under the pathological condition, SOD1 aggregates are associated with specific organelles such as the mitochondria and/or ER [34–37]. Since the tunicamycin-induced aggregates of mutant SOD1 were localized to the central and peripheral regions of the cytoplasm (Fig. 1E, H–J), we investigated the subcellular localization of these aggregates with organelle specific markers. Confocal microscopy analysis clearly showed colocalization of SOD1 and an ER retention signal

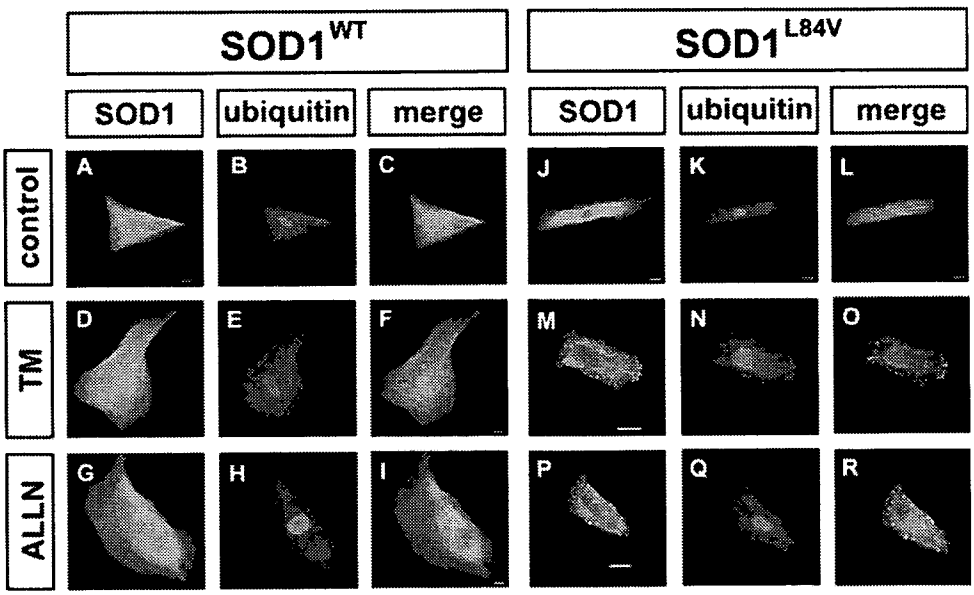

Figure 2. Ubiquitination of mutant SOD1 aggregates. (A–R) Colocalization assay with SOD1 and ubiquitin. SK-N-SH cells expressing wild-type SOD1 (A–I) or L84V SOD1 (J–R) were incubated with 1 μg/ml of tunicamycin (D–F, M–O), 4 μg/ml of ALLN (G–I, P–R), or no agents (A–C, J–L) for 24 h. Then the cells were fixed and stained with anti-SOD1 antibody (green; A, D, G, J, M, P) or anti-ubiquitin antibody (red; B, E, H, K, N, Q). Arrows indicate colocalization of SOD1 aggregates and ubiquitin. Scale bar = 20 μm. (S) Co-immunoprecipitation assay utilizing ubiquitin. SK-N-SH cells stably expressing wild-type and L84V SOD1 were transfected with a myc-tagged ubiquitin expression vector. After incubation with or without ALLN, cell lysates were prepared and assayed with anti-myc antibody of the immunoprecipitant with anti-FLAG antibody. Asterisk shows an ubiquitinated ladder that appeared after ALLN treatment of L84V SOD1-expressing cells. IgG bands are shown as loading controls.
doi:10.1371/journal.pone.0001030.g002

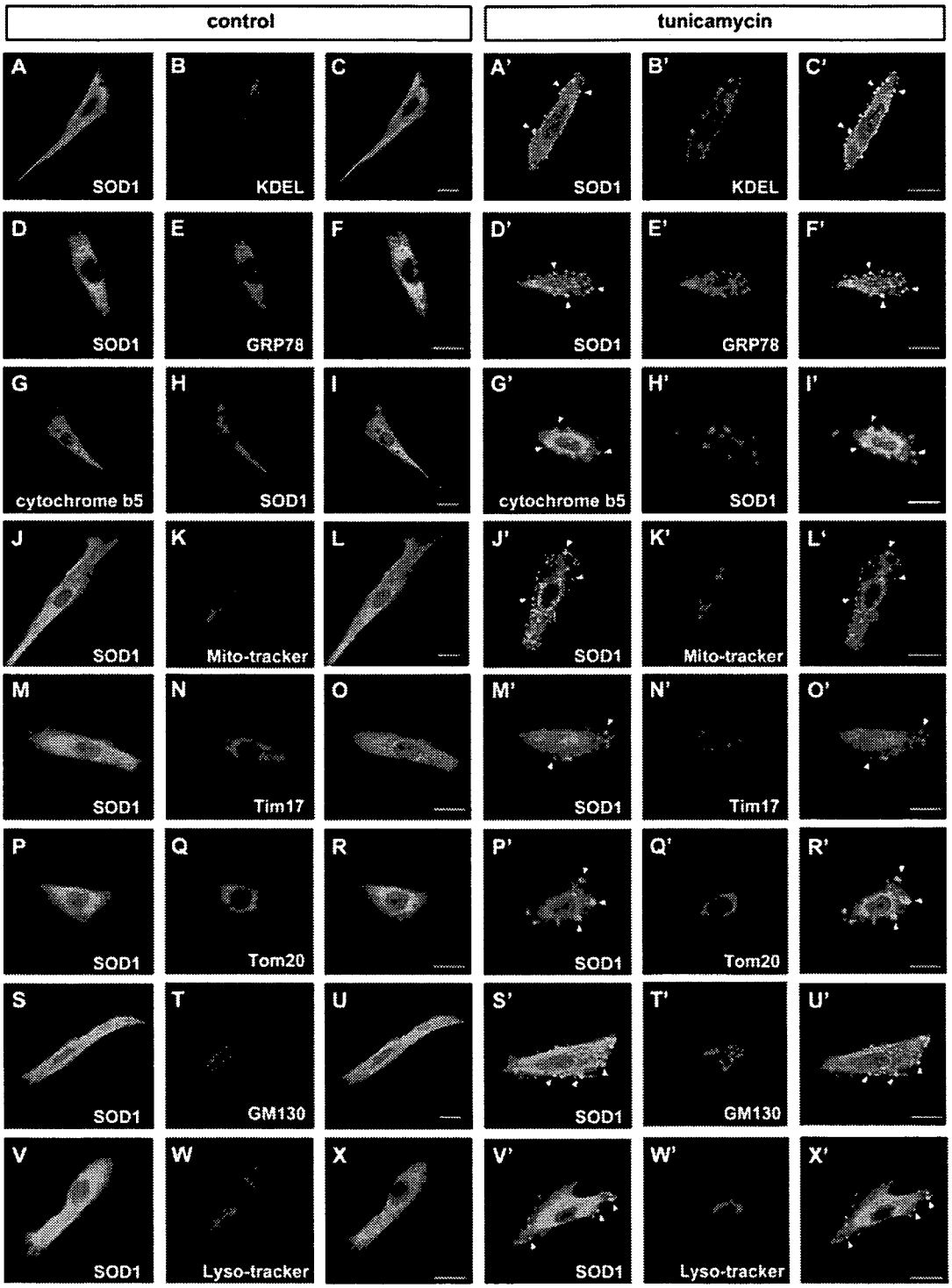

Figure 3. Positive translocation of SOD1 aggregates to ER, but not to the mitochondria, Golgi apparatus, or lysosomes. (**A–I, A'–I'**) Stress-dependent localization of SOD1 to the ER. L84V SOD1-expressing SK-N-SH cells were incubated for 24 h without (**A–I**) or with 1 μg/ml of tunicamycin (**A'–I'**). Then the cells were fixed and stained using an anti-SOD1 antibody (green; **A, D, A', D'**) and an anti-KDEL antibody (red; **B, B'**) or an anti-GRP78/BiP antibody (red; **E, E'**). GFP-cytochrome b5 were transfected to the cells and stained with anti-GFP (green; **G, G'**) and anti-SOD1 (red; **H, H'**) antibodies. Merged images (**C, F, I, C' F', I'**). The aggregates of SOD1 (arrowheads) are positive for KDEL, GRP78/BiP and cytochrome b5. (**J–R, J'–R'**) Analysis of SOD1 localization to the mitochondria. L84V SOD1-expressing SK-N-SH cells were treated as described in above. The locations of the mitochondria and SOD1 were visualized in L84V SOD1-expressing SK-N-SH cells using 100 nM Mito-tracker (red; **K, K'**), an anti-Tim17 antibody (red; **N, N'**) or an anti-Tom20 antibody (red; **Q, Q'**) and an anti-SOD1 antibody (green; **J, M, P, J', M', P'**). Merged images (**L, O, R, L', O', R'**). (**S–U, S'–U'**) Investigation of SOD1 localization to the Golgi apparatus. L84V SOD1-expressing SK-N-SH cells were treated as described in above. Then the cells were stained with anti-SOD1 antibody (green; **S, S'**) and anti-GM130 antibody (red; **T, T'**). Merged images (**U, U'**). (**V-X, V'-X'**) Analysis of the localization of SOD1 to the lysosomes. A GFP-tagged L84V SOD1 vector was transfected into L84V SOD1-expressing SK-N-SH cells. After 24 h of incubation with 1 μg/ml of tunicamycin, the cells were incubated for a further 30 min with 100 nM Lyso-tracker (red; **W, W'**) to visualize the lysosomes. GFP channel (**V, V'**) Merged images (**X, X'**). Scale bars = 20 μm. Arrowheads indicate aggregated SOD1.

doi:10.1371/journal.pone.0001030.g003

(KDEL) containing protein and GRP78/BiP, suggesting SOD1 localization in ER (Fig. 3A–F, A′–F′). In order to confirm the SOD1 colocalization with ER, we utilized GFP conjugated cytochrome b5, a typical C-terminal anchored ER membrane protein. As expected, SOD1 showed the positive staining with cytochrome b5, indicating mutant SOD1 localization to ER (Fig. 3G–I, G′–I′). In the absence of stress, ER was located to the perinuclear region. However, treatment with tunicamycin seemed to cause its relocation to an abnormal region near the cell periphery. The aberrant distribution of ER following tunicamycin treatment was not observed in cells expressing wild type SOD1 (Fig. S1C′, F′ and I′). These results suggest deterioration of ER function and localization due to aggregation of mutant SOD1.

In light of previous reports identifying mutant SOD1 colocalization to the mitochondria [34,35,37], we also examined the potential colocalization of mutant SOD1 with mitochondria. In contrast to the results with markers for ER, the SOD1 aggregates induced by tunicamycin did not colocalize with the mitochondria marker Mitotracker, with Tim17 which marks the mitochondrial inner membrane nor Tom20 which marks the mitochondrial outer membrane (Fig. 3J′–R′). The localization of these SOD1 aggregates also did not correspond with the Golgi apparatus or the lysosomes, which were stained by anti-GM130 antibody and Lyso-tracker, respectively (Fig. 3S′–X′).

Our previous results in figure 3C′, F′ and I′ revealed aberrant redistribution of ER membranes in tunicamycin-treated mutant SOD1 expressing cells to the cell periphery region. To directly visualize the localization of ER, we performed electron microscopic analysis of tunicamycin-stressed cells expressing mutant SOD1. Figure 4A and B showed abnormal aggregates of rough ER, sac-like structures with surface ribosomes, associated with numerous free ribosomes. Mutant SOD1 localization to these peripheral aggregates was confirmed by immunoelectron microscopy (Fig. 4C), implying defective functional activities of ER and free ribosomes in cells expressing mutant SOD1.

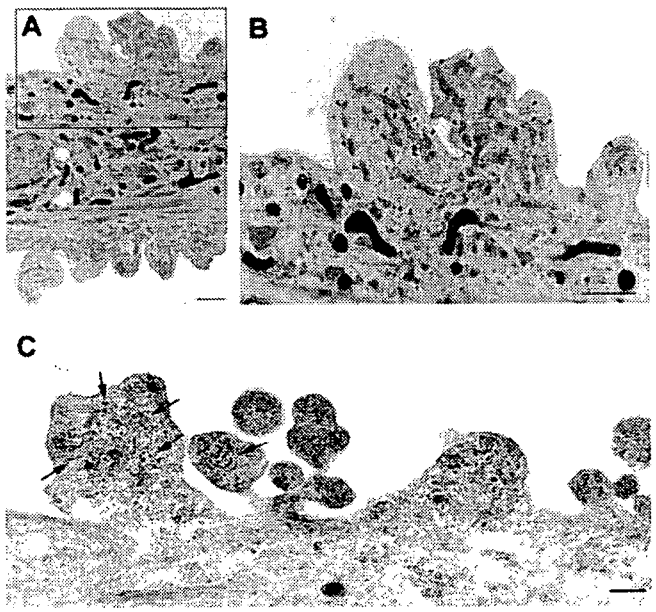

Figure 4. ER and SOD1 co-localization in peri-cytoplasmic membrane region. (A) Electron micrograph of L84V SOD1-expressing SK-N-SH cells after treatment with 1 μg/ml of tunicamycin for 24 h as described in Materials and Methods. (B) Enlargement of part of (A). Arrowheads indicate abnormal ER aggregates, where mutant SOD1 is localized as in Fig. 3C′ and 3E′. Scale bar = 1 μm. (C) SOD1 localization in peri-cytoplasmic membrane region. Cells were treated as described in (A) and immune electron micrograph was obtained as described in Materials and Methods. Arrows show SOD1 immunoreactive in ER.
doi:10.1371/journal.pone.0001030.g004

LBHI/Ast-HI-like Inclusions are induced by ER stress.

Wate et al. [28] reported that neuronal LBHI in G93A SOD1 transgenic mice are immune reactive for GRP78/BiP, an ER resident component of the UPR response. As shown in figures 3A′-I′ and 4C, mutant SOD1 localized to the ER following stress induction by tunicamycin. These SOD1 aggregates shared additional features with LBHI/Ast-HI, namely eosin positivity and ubiquitin immune reactivity. Those observations led us to consider whether ER stress would eventually induce the formation of full-fledged LBHI/Ast-HI. To test this hypothesis, we examined whether inclusion bodies containing mutant SOD1 developed in L84V SOD1-expressing cells subjected to ER stress. Consistent with this idea, eosinophilic hyaline inclusions (~10 to 20 μm in diameter) with a pale core, which are similar to neuronal LBHI/Ast-HI in the spinal cord of ALS patients harboring a SOD1 mutation, developed within 24 hrs of exposure to tunicamycin (Fig. 5A), but not in cells expressing wild type SOD1 (data not shown). In fact, the eosin-positive LBHI/Ast-HI-like hyaline inclusions (LHIs) were morphologically similar to the Ast-HI seen in the spinal cord of transgenic L84V SOD1 mice at the symptomatic stage (Fig. 5A and D). Furthermore, ultrastructual analysis revealed that the LHIs in neuroblastoma cells were composed of granule-coated fibrils (approximately 15–25 nm in diameter) and granular materials, which are the typical morpho-

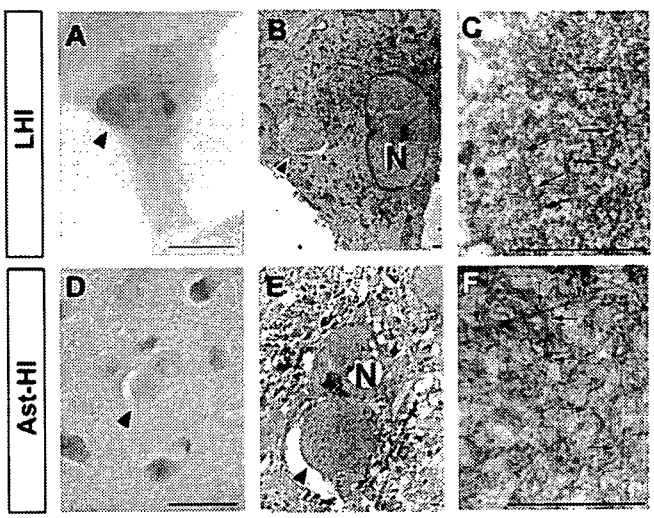

Figure 5. LHIs containing granule-coated fibrils are morphologically identical with Ast-HI from L84V transgenic mice. (A–F) Comparison of a LHI induced by ER stress in an L84V SOD1-expressing SK-N-SH cell (A–C) and Ast-HI in the spinal cord of a transgenic L84V SOD1 mouse (D–F). (A) An eosinophilic LHI in the cytoplasm of the SK-N-SH cell expressing L84V SOD1 cell was induced by treatment with 1 μg/ml of tunicamycin for 24 h (scale bar = 20 μm). (B) Electron micrograph of a hyaline inclusion (arrow) obtained by the direct epoxy resin-embedding method after decolorization of the HE-stained section shown in (A). N, nucleus; ×3000 (scale bar = 1 μm). (C) At a high magnification, the inclusion is composed of granule-coated fibrils (arrows) approximately 15–25 nm in diameter and granular materials. ×16000 (scale bar = 1 μm). (D) An eosinophilic Ast-HI from a transgenic L84V SOD1 mouse. (E) Electron micrograph of an Ast-HI obtained by the direct epoxy resin-embedding method mentioned in (B). N, nucleus; ×2000 (scale bar = 1 μm). (F) Enlargement of (E). ×16000 (scale bar = 1 μm). Note that the fibrils observed in (C) and (F) are ultrastructually identical.
doi:10.1371/journal.pone.0001030.g005

logical hallmarks of mutant SOD1-linked FALS, and were identical with the Ast-HI found in L84V SOD1 mice (Fig. 5C, F; [38]). These results suggest that LBHI/Ast-HI in FALS patients might be provoked by ER stress as we observed for LHIs.

We further explored the molecular similarity between the LHI and LBHI/Ast-HI, using double-label immunocytochemistry. As shown in figure 6A–D, LHIs induced by tunicamycin are immunopositive for anti-SOD1 and anti-ubiquitin antibodies, consistent with the LBHI/Ast-HI features. In the spinal cord of G93A SOD1 mutant mice at the symptomatic stage, neuronal LBHI show GRP78/BiP immunoreactive, suggesting the involvement of ER resident protein [28]. Therefore, we examined whether LHIs also contain ER resident protein. As expected, LHI showed anti-KDEL positivity, indicating the involvement of ER resident proteins such as calreticulin, GRP 94, PDI and GRP78/BiP in LHI development (Fig. 6E and F). Furthermore, Ast-HI in spinal cord of L84V SOD1 transgenic mice at symptomatic stage also showed KDEL positive (Fig. 6G and H), meaning that the principle features of these inclusions in neuroblastoma cells and the LBHI/Ast-HI of FALS patients are the same and implying LHI and LBHI/Ast-HI might develop in similar procedure.

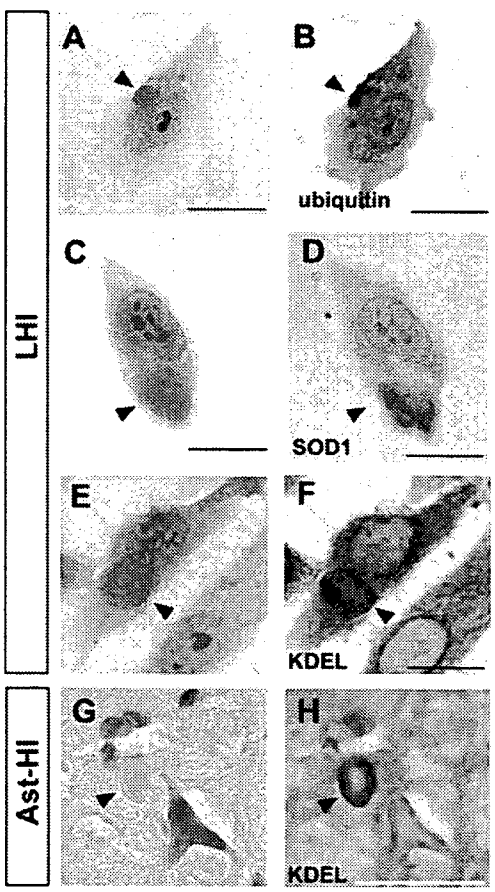

Figure 6. Positive immunoreactive against ubiquitin, SOD1 and KDEL of LHIs. (A–D) LHIs show immunoreactive against ubiquitin and SOD1. Eosinophilic LHIs in SK-N-SH cells (arrowheads in A and C) induced by tunicamycin were immunostained for ubiquitin (B) and SOD1 (D) after de-colorization. (E–H) KDEL immunoreactive in both LHI and Ast-HI. Eosinophilic LHI in SK-N-SH cells (arrowhead in E) and Ast-HI in spinal cord of L84V SOD1 mouse (arrowhead in G) were immunostained against anti-KDEL antibody after de-colorization (F, H). Scale bar = 20 μm

doi:10.1371/journal.pone.0001030.g006

Abnormal ER aggregated around peri-nuclear region with numerous free ribosomes at presymptomatic stage of Ast-HI in L84V SOD1 mice.

To further explore the relationship of LHI to the development of LBHI/Ast-HI in FALS patients with mutant SOD1, we performed ultrastructual examination of transgenic L84V SOD1 mice, which show neuronal LBHI and Ast-HI at symptomatic stage (Fig. 5D–F, 6G–H; [35]). We examined the mice at the presymptomatic stage in the hope of detecting precursors to hyaline inclusion bodies. In spinal cord neurons of the pre-symptomatic L84V SOD1 transgenic mice, we observed aberrant aggregation of electron-dense rough ER around the peri-nuclear region with numerous free ribosomes, which were suspected to be producing mutant SOD1 (Fig. 7). This suggests that the aberrant SOD1 fibrils observed in spinal neurons of these mice at later

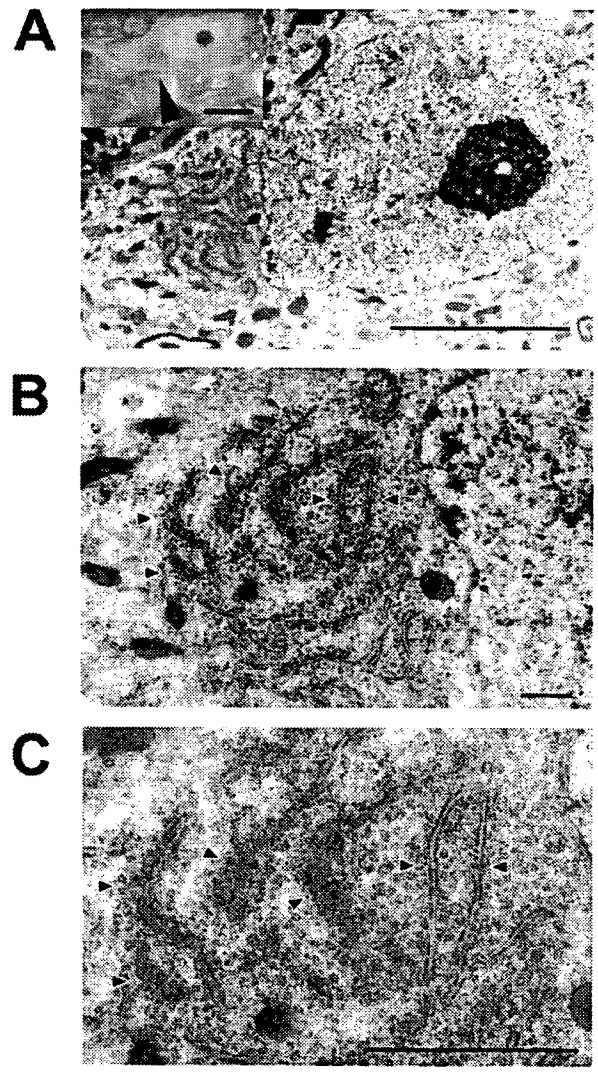

Figure 7. ER shows abnormal aggregation with numerous free ribosomes in L84V SOD1 mouse at presymptomatic stage. (A–C) Electron micrographs of a neuron obtained from an L84V SOD1 transgenic mouse containing ER aggregates. The inset in (A) shows a cytoplasmic inclusion-like structure (arrowhead) stained with toluidine blue. (A) ×3500 (scale bars = 20 μm). (B) ×8000 (scale bar = 1 μm). (C) ×15000 (scale bar = 1 μm). Arrowheads indicate abnormal ER aggregates.

doi:10.1371/journal.pone.0001030.g007